Supplementary Information

Divergent Catalytic Behaviors of Assembled Organogold(I) Clusters Derived from Enyne Cyclization

Qian Liu, Xiaoyi Zhai, Ruijun Jian, and Liang Zhao*

Key Laboratory of Bioorganic Phosphorus Chemistry and Chemical Biology (Ministry of Education), Department of Chemistry, Tsinghua University, Beijing 100084, China.

E-mail: zhaolchem@mail.tsinghua.edu.cn; Phone: +86-10-62786635.

Table of Contents

Synthesis of σ-aurated substrates 1a-1c, 3-3'.

Synthesis of 1a

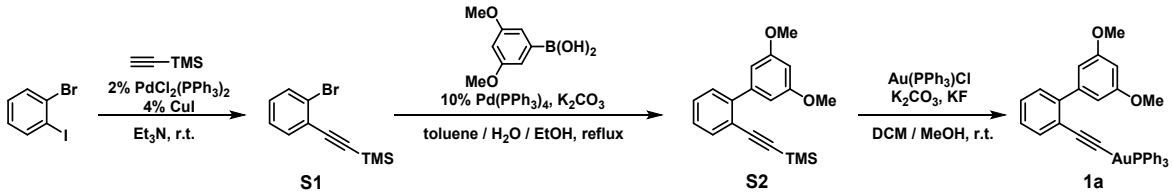

S1, S2 were prepared according to literature procedures.[1,2] **S2** (34.2 mg, 0.11 mmol) and $Au(PPh_3)Cl$ (49.5 mg, 0.1mmol) were dissolved in CH_2Cl_2 (4 ml). A methanol solution (1 mL) of KF (8.7 mg, 0.15 mmol) and K_2CO_3 (138.2 mg, 1 mmol) was then added to the solution under stirring at room temperature overnight. After removing the solvent by rotary evaporation under vacuum, the residual was re-dissolved in CH_2Cl_2 and filtered through celite. The filtrate was concentrated under reduced pressure, which was added dropwise into 50 mL petroleum ether under vigorous stirring. A pale-yellow precipitate **1a** was finally obtained. Yield: 81% (62.1 mg). ^{1}H-NMR (400 MHz, $CDCl_3$): δ (ppm) 7.66-7.63 (m, 1H), 7.55-7.42 (m, 15H), 7.40-7.36 (m, 1H), 7.27-7.22 (m, 2H), 7.03 (d, J = 2.4 Hz, 2H), 6.44 (t, J = 2.4 Hz, 1H), 3.84 (s, 6H). ^{13}C-NMR (100 MHz, $CDCl_3$): δ (ppm) 160.05, 143.31, 138.04, 136.62, 134.57, 134.31, 131.66, 131.64, 130.17, 129.62, 129.54, 129.28, 129.24, 129.17, 128.67, 128.55, 127.10, 126.96, 123.12, 123.10, 107.53, 103.48, 103.22, 100.69 and 55.62. ^{31}P-NMR (162 MHz, $CDCl_3$): δ (ppm) 42.83.

Synthesis of 1b

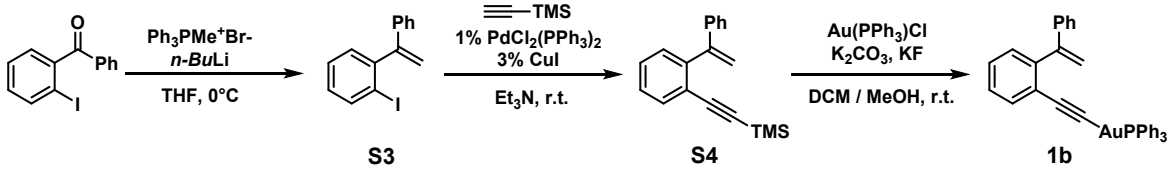

S3 was prepared according to literature procedures.[3] To a stirred mixture of **S3** (306.2 mg, 1.0 mmol), $PdCl_2(PPh_3)_2$ (7 mg, 1 mol %) and CuI (5.7 mg, 3 mol %) in Et_3N (1 mL) and THF (5 mL) at room temperature under an argon atmosphere, trimethylsilylacetylene (0.28 mL, 2.0 mmol, 2 equiv.) was added dropwise. The reaction mixture was stirred for 12 h at room temperature. The reaction mixture was filtered through Celite and the solvent was removed by rotary evaporation. The residue was treated with water and extracted with CH_2Cl_2. The combined organic phases were washed with brine, dried over anhydrous Na_2SO_4 and the solvent was removed under vacuum. The residue was purified by flash column chromatography on silica gel (petroleum ether as eluent) to afford **S4**. Yield: 92% (254.3 mg). The spectra are consistent with the compound reported in the literature.[4] ^{1}H-NMR (400 MHz, $CDCl_3$): δ (ppm) 7.57-7.52 (m, 1H), 7.41-7.29 (m, 8H), 5.78 (d, J = 1.6 Hz, 1H), 5.42 (d, J = 1.6 Hz, 1H), 0.06 (s, 9H).

The synthetic procedures for **1b** is similar with that of **1a** but with **S4** (30.4 mg, 0.11 mmol) instead of **S2**. A pale-yellow precipitate was finally obtained. Yield: 85% (61.9 mg). ^{1}H-NMR (400 MHz, $CDCl_3$): δ (ppm) 7.56-7.42 (m, 23H), 7.17-7.12 (m, 3H), 5.22 (s, 2H). ^{13}C-NMR (100 MHz, $CDCl_3$): δ (ppm) 149.09, 144.34, 141.96, 138.06, 136.63, 134.50, 134.36, 134.00, 131.58, 131.56, 130.31, 129.76, 129.65, 129.21, 129.10, 127.99, 127.74, 127.05, 126.54, 124.43, 124.41, 116.52, 102.91 and 102.64. ^{31}P-NMR (162 MHz, $CDCl_3$): δ (ppm) 42.84.

Synthesis of 1c

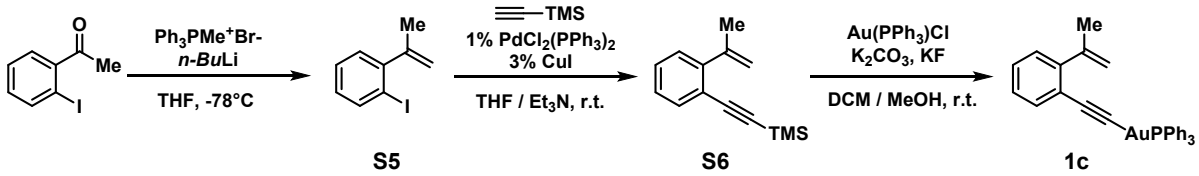

S5, **S6** were prepared according to literature procedures.[5] The synthetic procedures for 1c is similar with that of 1a but with **S6** (22.4 mg, 0.11 mmol) instead of **S2**. A white precipitate was collected by filtration. Yield: 83% (54.8 mg). ^{1}H-NMR (400 MHz, $CDCl_3$): δ (ppm) 7.58-7.4 (m, 16H), 7.18-7.12 (m, 3H), 5.23 (s, 2H), 2.30 (s, 3H). ^{13}C-NMR (100 MHz, $CDCl_3$): δ (ppm) 146.09, 146.00, 134.51, 134.37, 131.61, 131.59, 130.27, 129.71, 129.26, 129.15, 127.71, 126.75, 126.50, 122.63, 115.46,103.29, 103.02 and 23.52. ^{31}P-NMR (162 MHz, $CDCl_3$): δ (ppm) 42.83.

Synthesis of 1b'

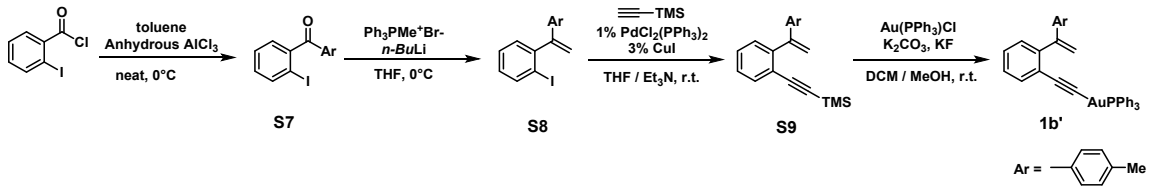

S7, **S8**, **S9** were prepared according to literature procedures.[6-8] The synthetic procedures for **1b'** is similar with that of **1a** but with **S9** (31.9 mg, 0.11 mmol) instead of **S2**. A pale yellow precipitate was finally obtained. Yield: 77% (57.3 mg). ^{1}H-NMR (400 MHz, $CDCl_3$): δ (ppm) 7.66-7.63 (m, 1H), 7.54-7.42 (m, 16H), 7.40-7.36 (m, 1H), 7.27-7.2 (m, 1H), 7.03-7.02 (d, J = 8 Hz, 2H), 5.75 (d, J = 1.2 Hz, 1H), 5.51 (d, J = 1.2 Hz, 1H), 2.25 (s, 3H). ^{13}C-NMR (100 MHz, $CDCl_3$): δ (ppm) 148.82, 144.54, 137.75, 136.62, 134.35, 134.03, 131.57, 131.54, 129.76, 129.59, 129.21, 129.16, 129.10, 128.68, 127.62, 126.93, 126.49, 124.39, 124.36, 115.71, 102.91, 102.65 and 21.27. ^{31}P-NMR (162 MHz, $CDCl_3$): δ (ppm) 42.82.

Synthesis of 3-3'

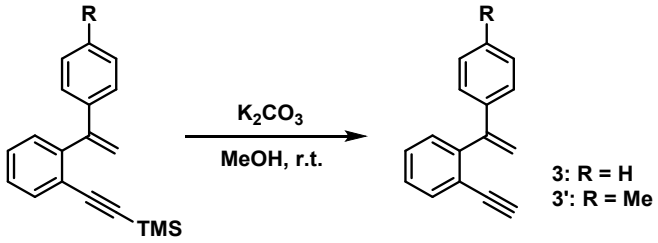

S4/**S9** (1 mmol) and K_2CO_3 (691, 5 mmol) were mixed together in MeOH (10 mL). The solution was left under stirring for 2 h at room temperature. Then it was hydrolyzed with water (10 mL) and extracted with CH_2Cl_2. The combined organic phases were washed with brine, dried over anhydrous Na_2SO_4 and the solvent was removed under vacuum. The residue was purified by flash column chromatography on silica gel (petroleum ether as eluent) to afford **3**/**3'**. Yield: 85% (173.6 mg) for **3** and 81% (176.8 mg) for **3'**. NMR data were consistent with that reported in literature.[3,8]

Kinetic monitoring of the catalytic reactions.

In an NMR tube, enyne substrate **3** (3.7 mg, 0.018 mmol), clusters **2a**-**2d** (0.00054 mmol) and internal standard 1,3,5-trimethoxybenzene (1 mg, 0.006 mmol) were combined in CD_2Cl_2 (0.5 mL) at 293K. The disappearance of **3** was monitored by the ^{1}H NMR signal at 2.97 ppm and then the integrations of proton signals were converted into concentrations to obtain kinetic curves.

X-ray crystallographic analysis.

Single-crystal X-ray data for **2a**, **2b**, **2c** and **2d** was collected at 100 K, 173K, 293K, 293K respectively, with Cu-Kα radiation (λ = 1.54178 Å) on a Rigaku Saturn 724/724+ CCD diffractometer with frames of oscillation range 0.5°. The selected crystal was mounted onto a nylon loop in poly-isobutene and immersed in a low-temperature stream of dry nitrogen gas during data collection. All structures were solved by direct methods, and non-hydrogen atoms were located from difference Fourier maps. Non-hydrogen atoms were subjected to anisotropic refinement by full-matrix least-squares on F^2 using the SHELXTL program[9] and Olex2 program[10] unless otherwise noted. The diffused electron density in the remaining void was treated by SQUEEZE program on the PLATON platform.[11] All figures were drawn by using Diamond program.

Crystal data for 2a (CCDC-2286449): $C_{92}H_{72}Au_4F_{12}N_2O_{10}P_4S_4$, M = 2633.50, triclinic, space group *P-1* (No. 2), a = 15.3967(2) Å, b = 23.3887(2) Å, c = 27.0694(3) Å, α = 90.7460(10)°, β = 91.7370(10)°, γ = 91.3300(10)°, V = 9739.91(19) Å^3, Z = 4, T = 100.03(10) K, D_c = 1.796 g cm^{-3}. The structure, refined on F^2, converged for 60249 unique reflections and 52739 observed reflections with $I > 2\sigma(I)$ to give R_1 = 9.29% and wR_2 = 25.56% and a goodness-of-fit = 1.068. The SQUEEZE procedure of PLATON was used in the processing of **2a**. **2a** was refined as a two-component twin.

Crystal data for 2b (CCDC-2286452): $C_{178}H_{130}Au_{11}F_{18}N_3O_{12}P_6S_6$, M = 5389.65, monoclinic, space group *C2/c* (No. 15), a = 29.4994(3) Å, b = 19.4956(2) Å, c = 33.2461(3) Å, α = 90°, β = 100.7470(10)°, γ = 90°, V = 18784.7(3) Å^3, Z = 4, T = 173(2) K, D_c = 1.906 g cm^{-3}. The structure, refined on F^2, converged for 19076 unique reflections (R_{int} = 0.0414) and 17707 observed reflections with $I > 2\sigma(I)$ to give R_1 = 3.42% and wR_2 = 8.85% and a goodness-of-fit = 1.028. The SQUEEZE procedure of PLATON was used in the processing of **2b**.

Crystal data for 2c (CCDC-2286453): $C_{284}H_{216}Au_{28}F_{24}N_4O_{16}P_8S_8$, M = 10416.16, orthorhombic, space group *C2/c* (No. 15), a = 47.3293(7) Å, b = 20.0353(5) Å, c = 41.2327(6) Å, α = 90°, β = 114.081(2)°, γ = 90°, V = 35696.4(13) Å^3, Z = 4, T = 293(2) K, D_c = 1.730 g cm^{-3}. The structure, refined on F^2, converged for 36215 unique reflections (R_{int} = 0.0526) and 25596 observed reflections with $I > 2\sigma(I)$ to give R_1 = 5.91% and wR_2 = 18.09% and a goodness-of-fit = 1.060. Four counterions were highly disordered and could not be reasonably located. The SQUEEZE procedure of PLATON was used in the processing of **2c**.

Crystal data for 2d (CCDC-2286454): $C_{190}H_{135}Au_{14}F_{12}N_2O_8P_5S_4$, M = 5842.61, triclinic, space group *P-1* (No. 2), a = 16.0520(4) Å, b = 18.4672(5) Å, c = 33.1755(8) Å, α = 84.197(2)°, β = 78.827(2)°, γ = 76.291(2)°, V = 9357.4(4) Å^3, Z = 2, T = 293(2) K, D_c = 2.074 g cm^{-3}. The structure, refined on F^2, converged for 31332 unique reflections (R_{int} = 0.0881) and 23694 observed reflections with $I > 2\sigma(I)$ to give R_1 = 6.58% and wR_2 = 18.39% and a goodness-of-fit = 1.031. The SQUEEZE procedure of PLATON was used in the processing of **2d**. There is one A alert of "Check Calcd Resid. Dens. 1.10Ang From Au0A" can be ascribed to the Fourier truncation error induced by the metal atom.

Supplementary Figures

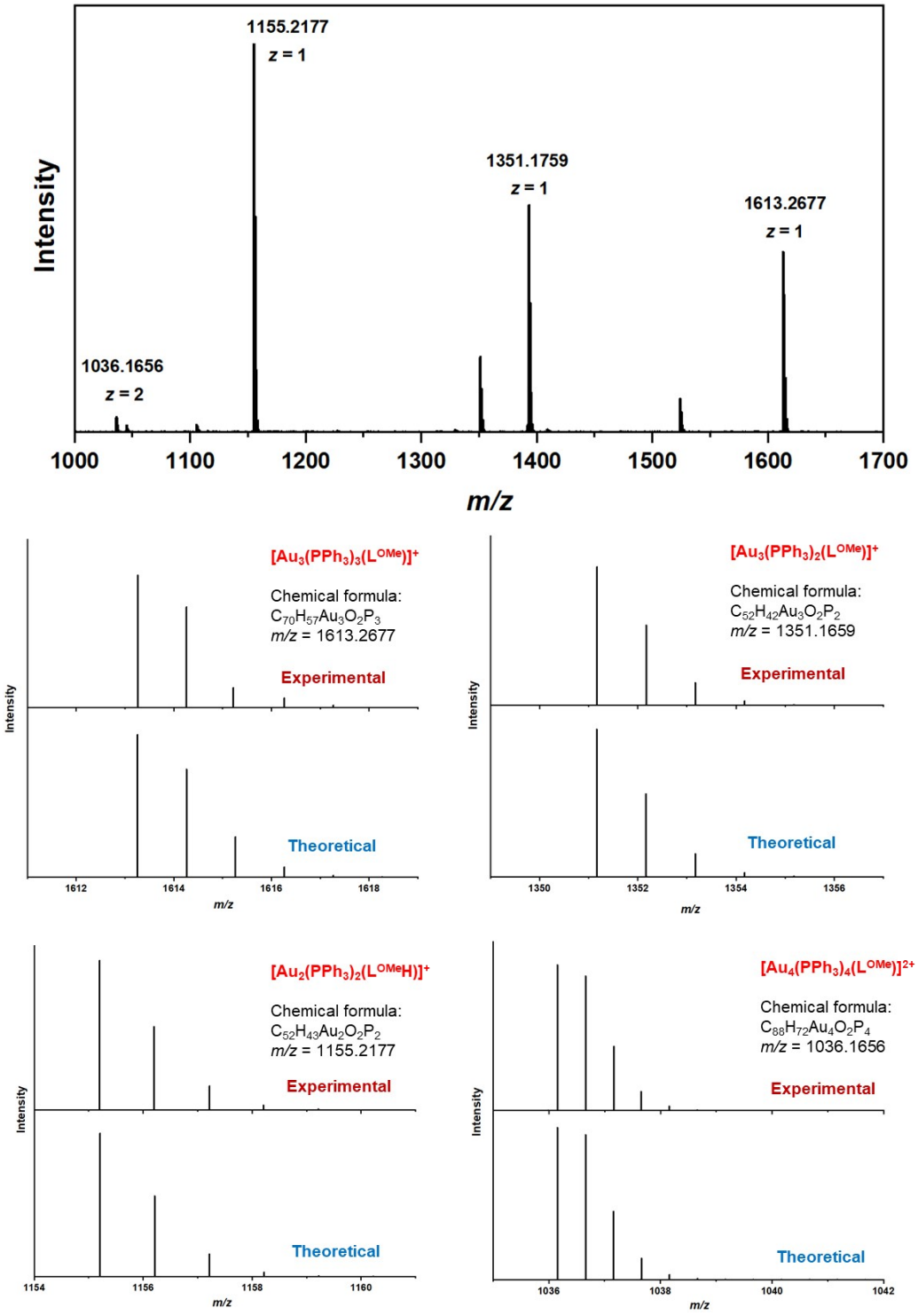

Fig. S1 The *in situ* electrospray ionization mass spectroscopy (ESI-MS) spectra of the reaction between **1a** and one equivalent $Au(PPh_3)(NTf_2)$ in 1,2-dichloroethane.

Calcd. for $C_{70}H_{57}Au_3O_2P_3$ 1613.2568 ($[Au_3(PPh_3)_3(L^{OMe})]^+$), found 1613.2677;

Calcd. for $C_{52}H_{42}Au_3O_2P_2$ 1351.1657 ($[Au_3(PPh_3)_2(L^{OMe})]^+$), found 1351.1759;

Calcd. for $C_{52}H_{43}Au_2O_2P_2$ 1155.2064 ($[Au_2(PPh_3)_2(L^{OMe}H)]^+$), found 1155.2177;

Calcd. for $C_{88}H_{72}Au_4O_2P_4$ 1036.1567 ($[Au_4(PPh_3)_4(L^{OMe})]^{2+}$), found 1036.1656.

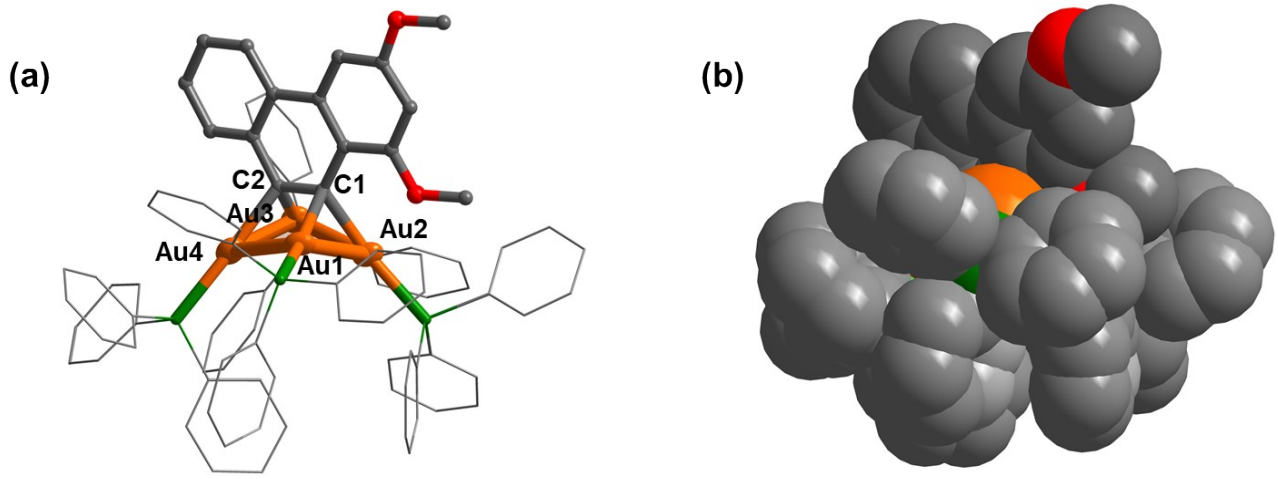

Fig. S2 (a) Crystal structure of complex **2a**. Hydrogen atoms, peripheral NTf_2^- counterions are omitted for clarity. Color coding: Au, orange; C, gray; P, green. Selected bond lengths (Å): Au1-Au2 2.7825(8); Au1-Au4 3.0472(8); Au2-Au3 2.9791(7); Au3-Au4 2.7859(8); Au1-C1 2.214(12); Au2-C1 2.125(14); Au3-C2 2.177(13); Au4-C2 2.108(14). (b) Space-filling model of **2a**.

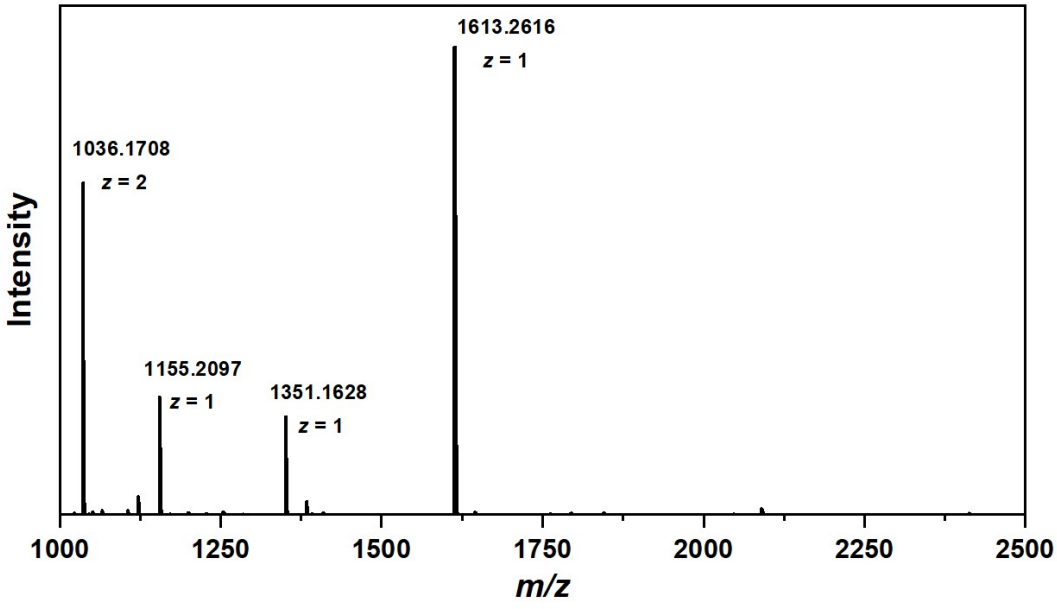

Fig. S3 High resolution ESI-MS spectra of complex **2a** in 1,2-dichloroethane.
Calcd. for $C_{88}H_{72}Au_4O_2P_4$ 1036.1567 ($[Au_4(PPh_3)_4(L^{OMe})]^{2+}$), found 1036.1708.

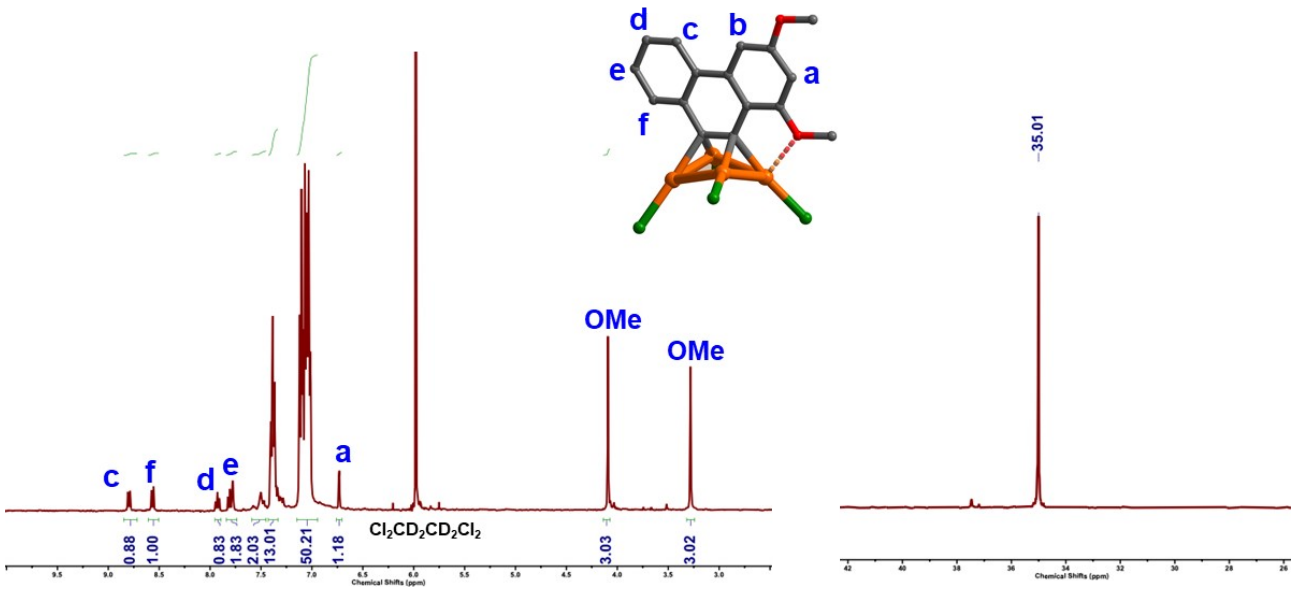

Fig. S4 ^{1}H and ^{31}P NMR spectra of complex **2a** in $Cl_2CD_2CD_2Cl_2$. Only one peak in ^{31}P NMR spectrum illustrates that there is rapid exchange of $[Au(PPh_3)]^+$ units in solution.

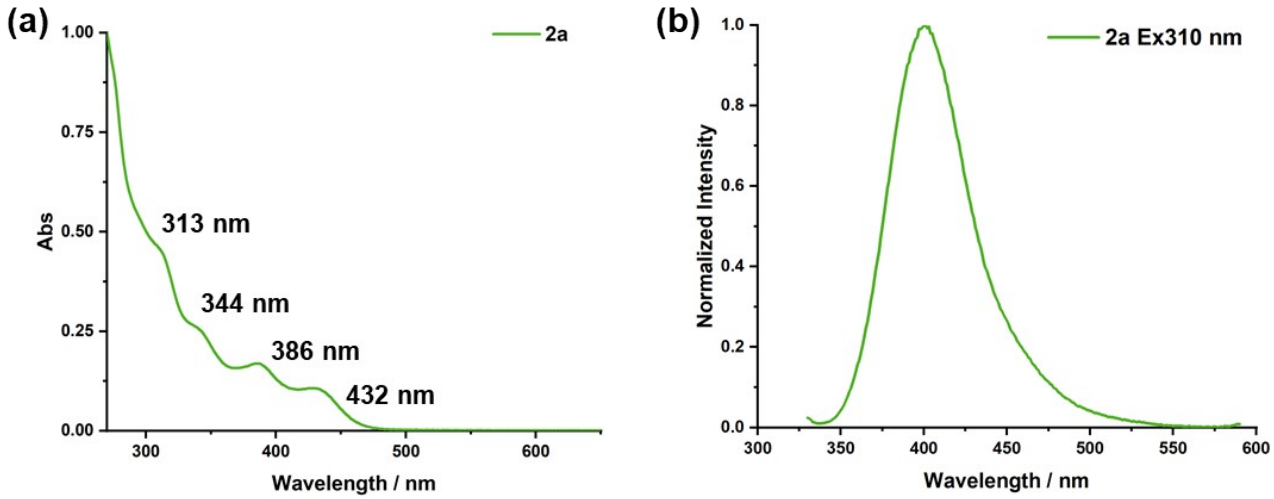

Fig. S5 UV-vis (a) and emission (b) spectra of complex **2a** in 1,2-dichloroethane.

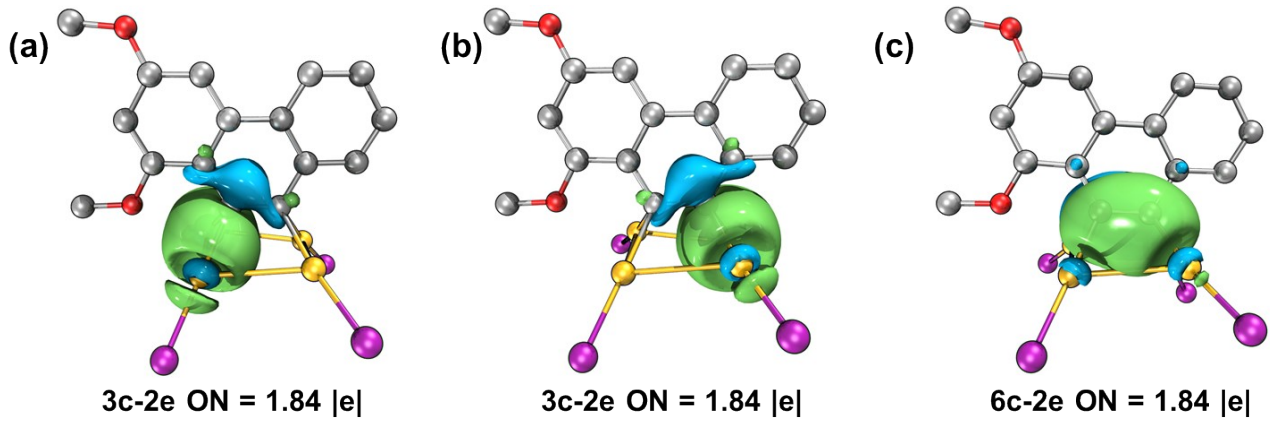

Fig. S6 AdNDP analysis of **2a** (isovalue: 0.03). Therein, the PPh_3 ligands were simplified as PH_3 and the effect of proton on the organic skeleton was neglected. The two degenerate 3*c*−2*e* bonds mainly comprise 2*s*, 2*p* orbitals of central dicarbon (19.2 and 57.3%, respectively) and 6*s* orbitals of digold (8.8 and 10.8%, respectively). The 6*c*−2*e* bonds mainly comprise 2*p* orbitals of central dicarbon (46.5 and 43.1%, respectively) and 6*s* orbitals of four gold atoms (about 2.0% each).

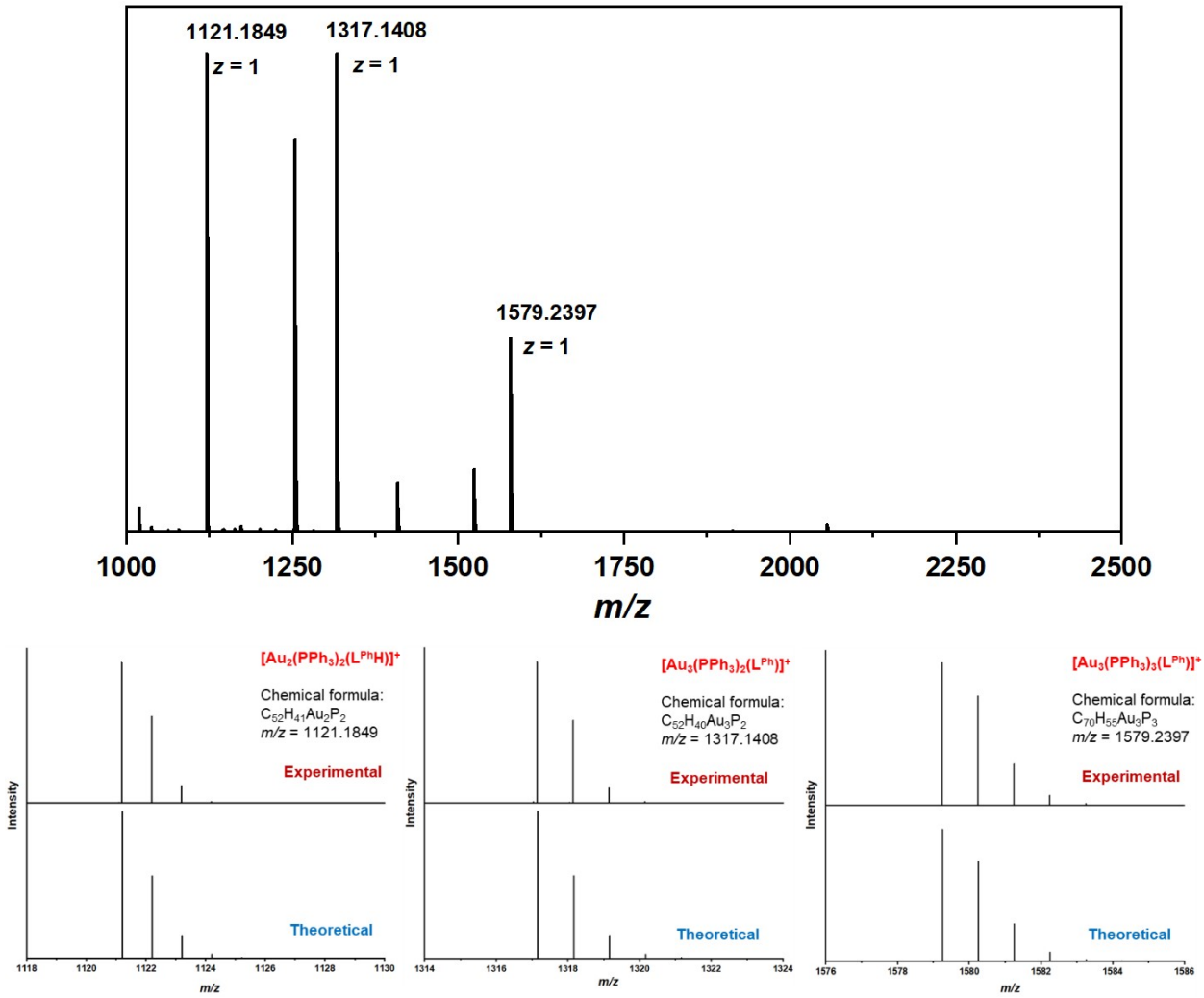

Fig. S7 The *in situ* ESI-MS spectra of the reaction between **1b** and three equivalents $Au(PPh_3)(NTf_2)$ in 1,2-dichloroethane.

Calcd. for $C_{52}H_{41}Au_2P_2$ 1121.2009 ($[Au_2(PPh_3)_2(L^{Ph}H)]^+$), found 1121.1849;

Calcd. for $C_{52}H_{40}Au_3P_2$ 1317.1596 ($[Au_3(PPh_3)_2(L^{Ph})]^+$), found 1317.1408;

Calcd. for $C_{70}H_{55}Au_3P_3$ 1579.2513 ($[Au_3(PPh_3)_3(L^{Ph})]^+$), found 1579.2397.

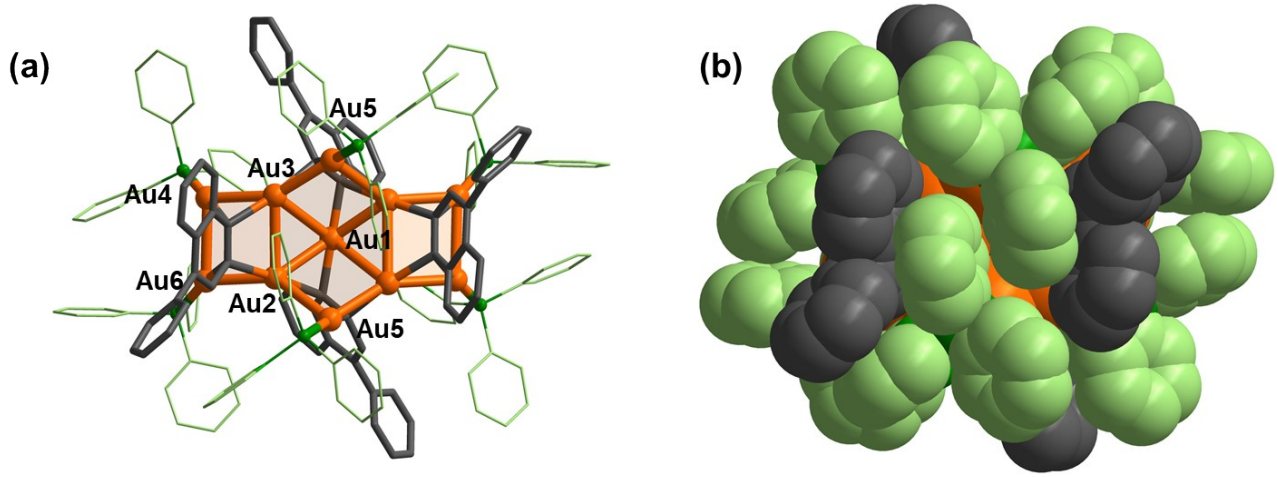

Fig. S8 (a) Crystal structure of complex **2b**. Hydrogen atoms, peripheral NTf_2^- counterions are omitted for clarity. Color coding: Au, orange; C, gray; PPh_3, green. Selected bond lengths (Å): Au1-Au2 2.7006(2); Au1-Au3 3.0766(2); Au2-Au3 3.0880(3); Au2-Au5 3.0413(3); Au2-Au6 2.7033(3); Au3-Au4 2.7141(3); Au3-Au5 2.7385(3); Au4-Au6 3.0719(3). (b) Space-filling model of **2b**.

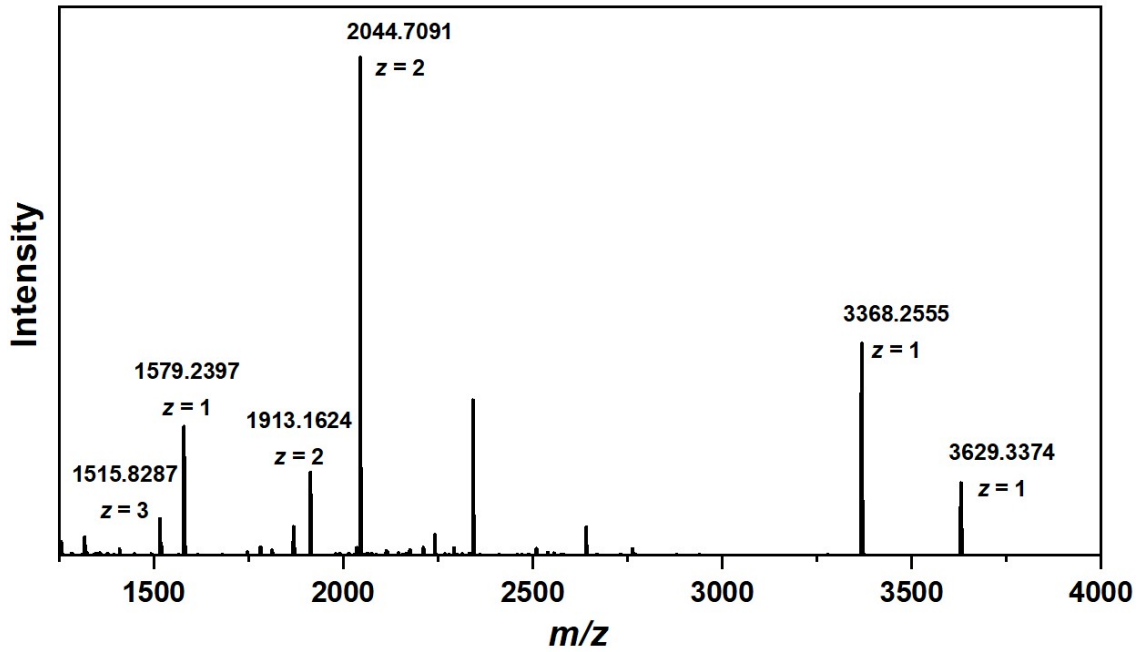

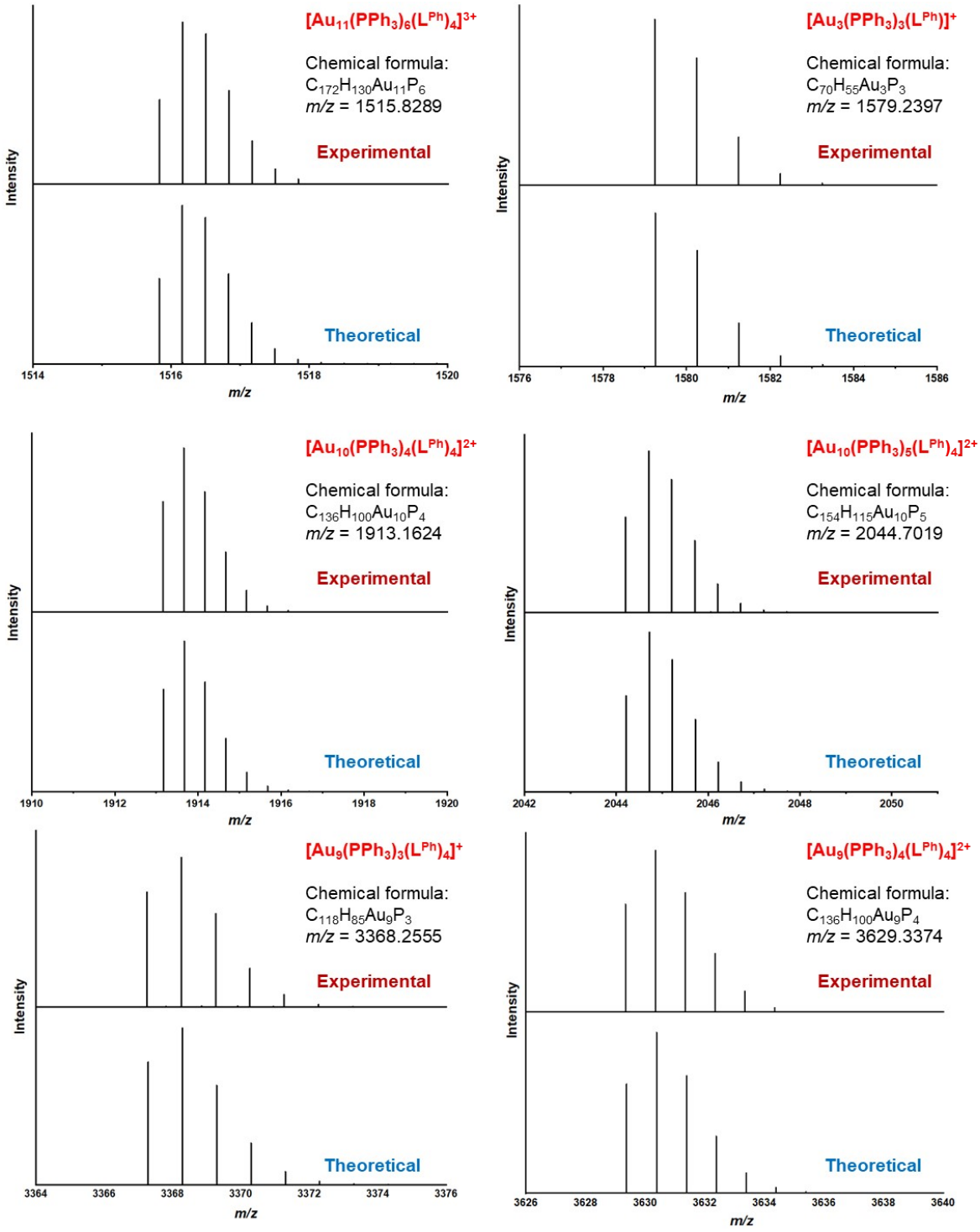

Fig. S9 High resolution ESI-MS spectra of complex **2b** in 1,2-dichloroethane.

Calcd. for $C_{172}H_{130}Au_{11}P_6$ 1515.8306 ($[Au_{11}(PPh_3)_6(L^{Ph})_4]^{3+}$), found 1515.8289;

Calcd. for $C_{70}H_{55}Au_3P_3$ 1579.2513 ($[Au_3(PPh_3)_3(L^{Ph})]^{+}$), found 1579.2397;

Calcd. for $C_{136}H_{100}Au_{10}P_4$ 1913.1710 ($[Au_{10}(PPh_3)_4(L^{Ph})_4]^{2+}$), found 1913.1624;

Calcd. for $C_{154}H_{115}Au_{10}P_5$ 2044.2166 ($[Au_{10}(PPh_3)_5(L^{Ph})_4]^{2+}$), found 2044.7019;

Calcd. for $C_{118}H_{85}Au_9P_3$ 3368.2932 ($[Au_9(PPh_3)_3(L^{Ph})_4]^{+}$), found 3368.2555;

Calcd. for $C_{136}H_{100}Au_9P_4$ 3629.3765 ($[Au_9(PPh_3)_4(L^{Me})_4]^{+}$), found 3629.3374.

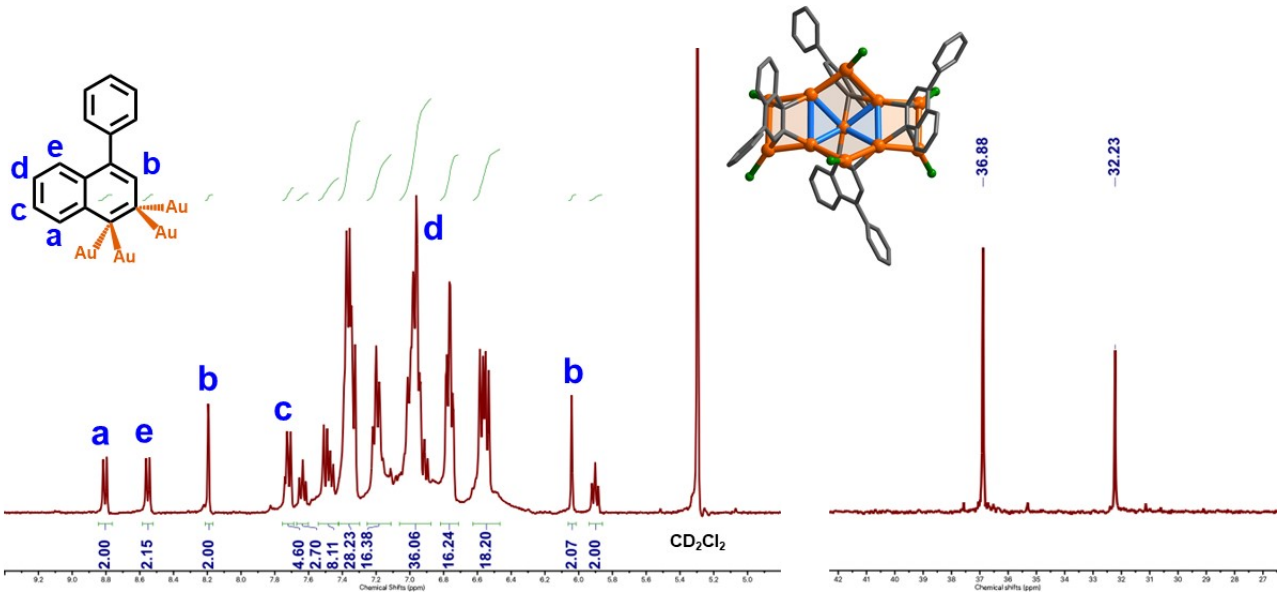

Fig. S10 ^{1}H and ^{31}P NMR spectra of complex **2b** in CD_2Cl_2.

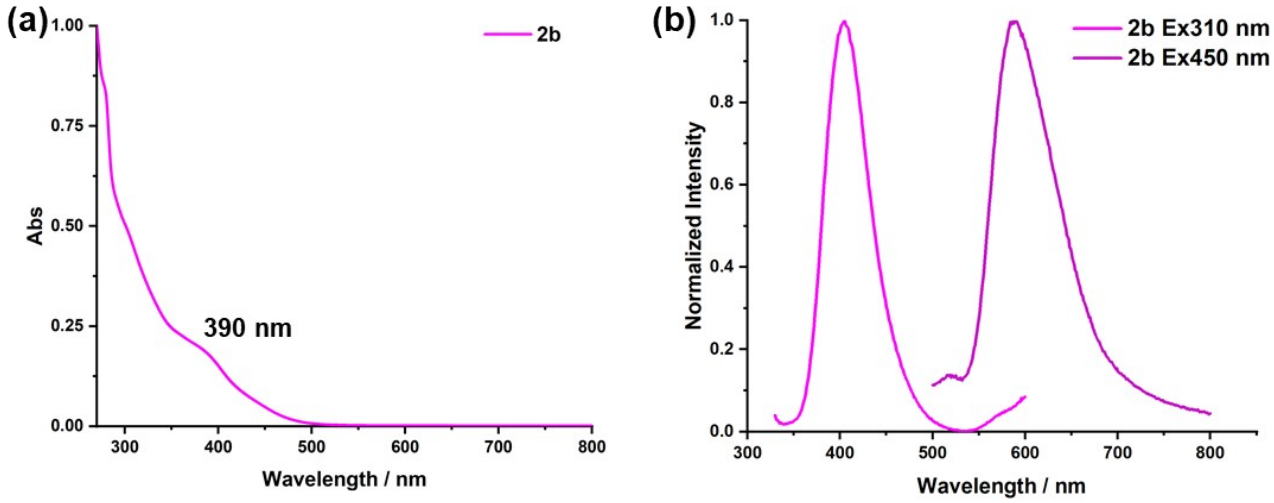

Fig. S11 UV-vis (a) and emission (b) spectra of complex **2b** in 1,2-dichloroethane.

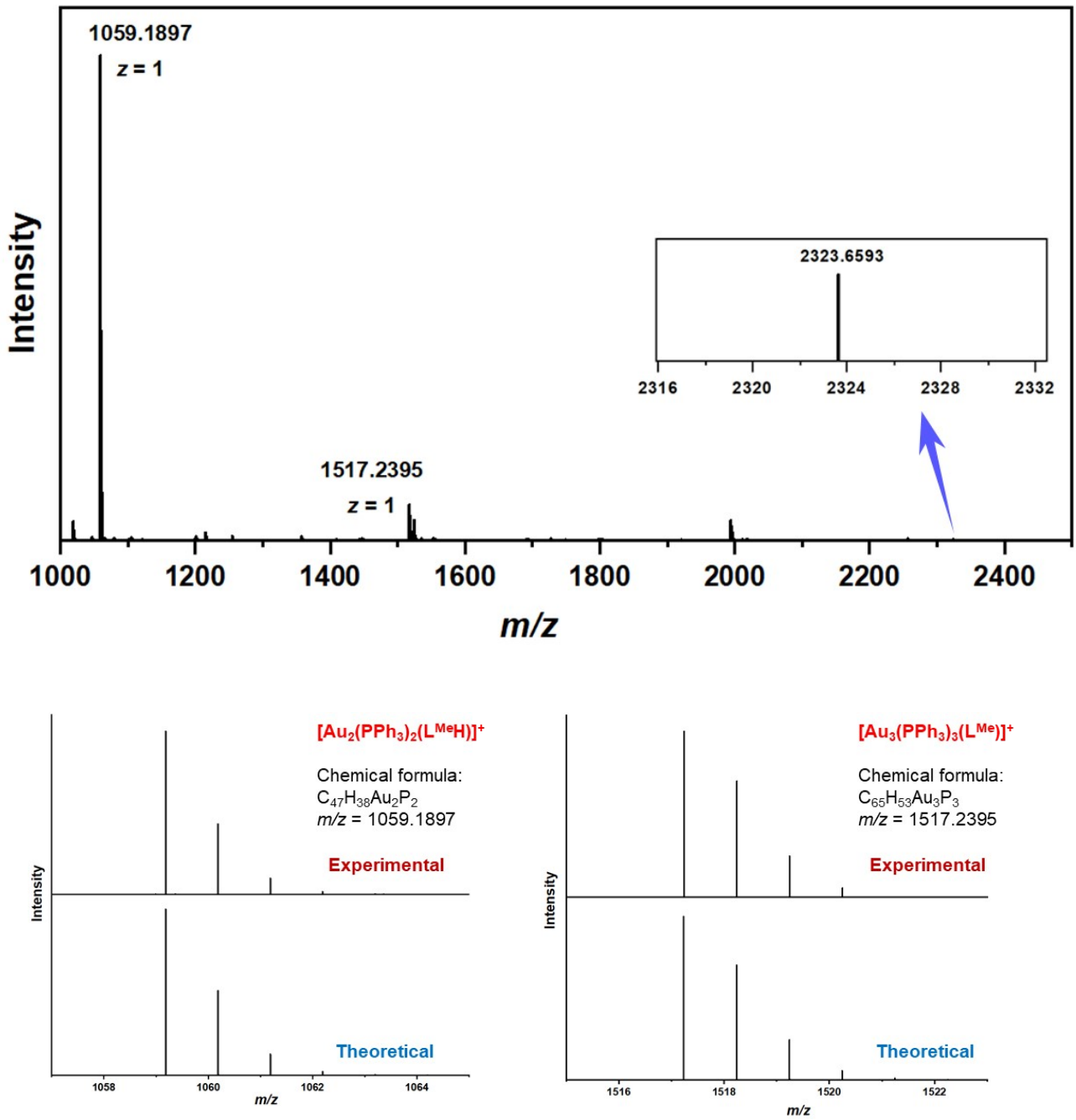

Fig. S12 High resolution ESI-MS spectra of the reaction between **1c** and three equivalents $Au(PPh_3)(NTf_2)$ in 1,2-dichloroethane.

Calcd. for $C_{147}H_{38}Au_2P_2$ 1059.1853 ($[Au_2(PPh_3)_2(L^{Me}H)]^+$), found 1059.1897;

Calcd. for $C_{65}H_{53}Au_3P_3$ 1517.2351 ($[Au_3(PPh_3)_3(L^{Me})]^+$), found 1517.2395.

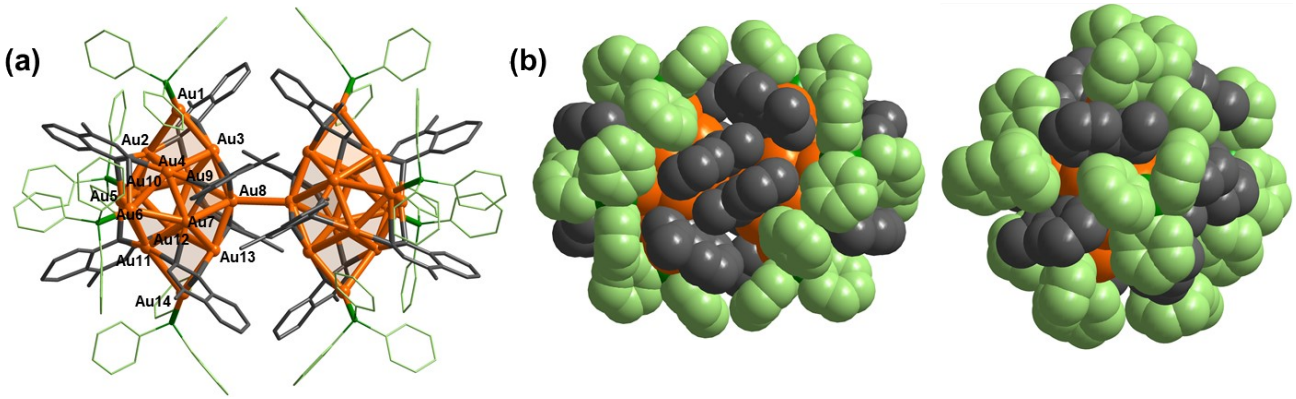

Fig. S13 (a) Crystal structure of complex **2c**. Hydrogen atoms, peripheral NTf_2^- counterions are omitted for clarity. Color coding: Au, orange; C, gray; PPh_3, green. Selected bond lengths (Å): Au1-Au2 3.1930(8); Au1-Au3 2.7002(6); Au1-Au4 3.546; Au2-Au3 3.518; Au2-Au4 3.2087(9); Au2-Au5 2.8046(7); Au2-Au10 2.8913(9); Au3-Au4 3.0682(7); Au3-Au8 2.6841(6); Au3-Au9 2.9897(8); Au4-Au6 2.7410(7); Au4-Au7 2.7269(6); Au5-Au10 2.8828(11); Au5-Au6 2.9011(11); Au5-Au11 2.7989(7); Au6-Au7 2.9308(7); Au6-Au11 2.8861(9); Au7-Au8 3.1686(7); Au7-Au13 3.0030(7); Au8-Au9 3.1638(7); Au8-Au13 2.6774(6); Au9-Au10 2.9945(7); Au9-Au12 2.7120(6); Au10-Au12 2.7464(7); Au11-Au12 3.2249(9); Au11-Au13 3.505; Au11-Au14 3.1106(7); Au12-Au13 3.0934(7); Au12-Au14 3.490; Au13-Au14 2.6900(6). (b) Space-filling model of **2c**, indicating the π–π stacking of methylnaphthalene and the steric hindrance of the peripheral ligand is responsible for the loss of one-fold C-Au bond.

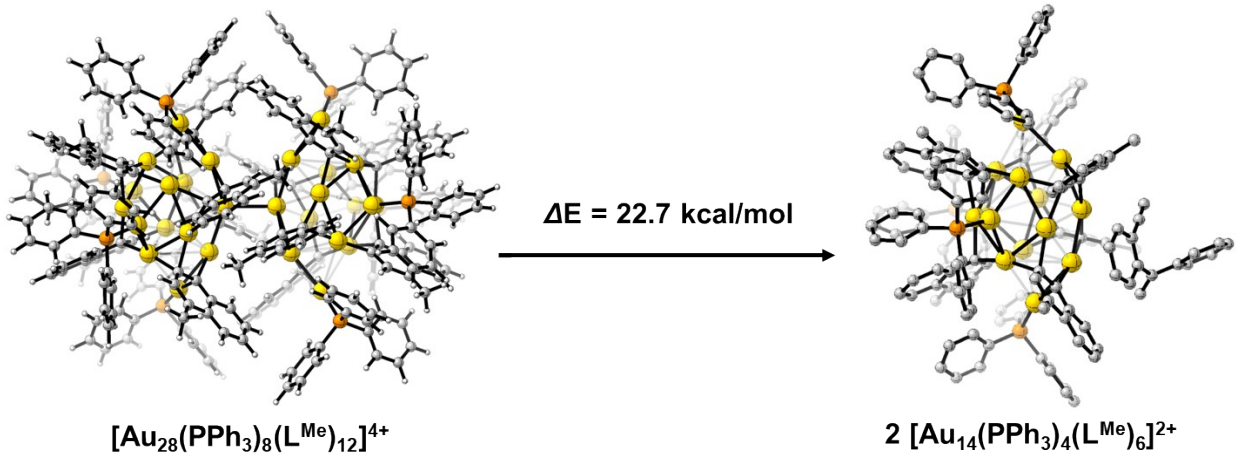

Fig. S14 DFT calculation for the energy of the dissociation of Au_{28} to $^{Me}Au_{14}$. This can be seen as the energy of breaking one Au-Au bond and two-fold π-π stacking interaction.

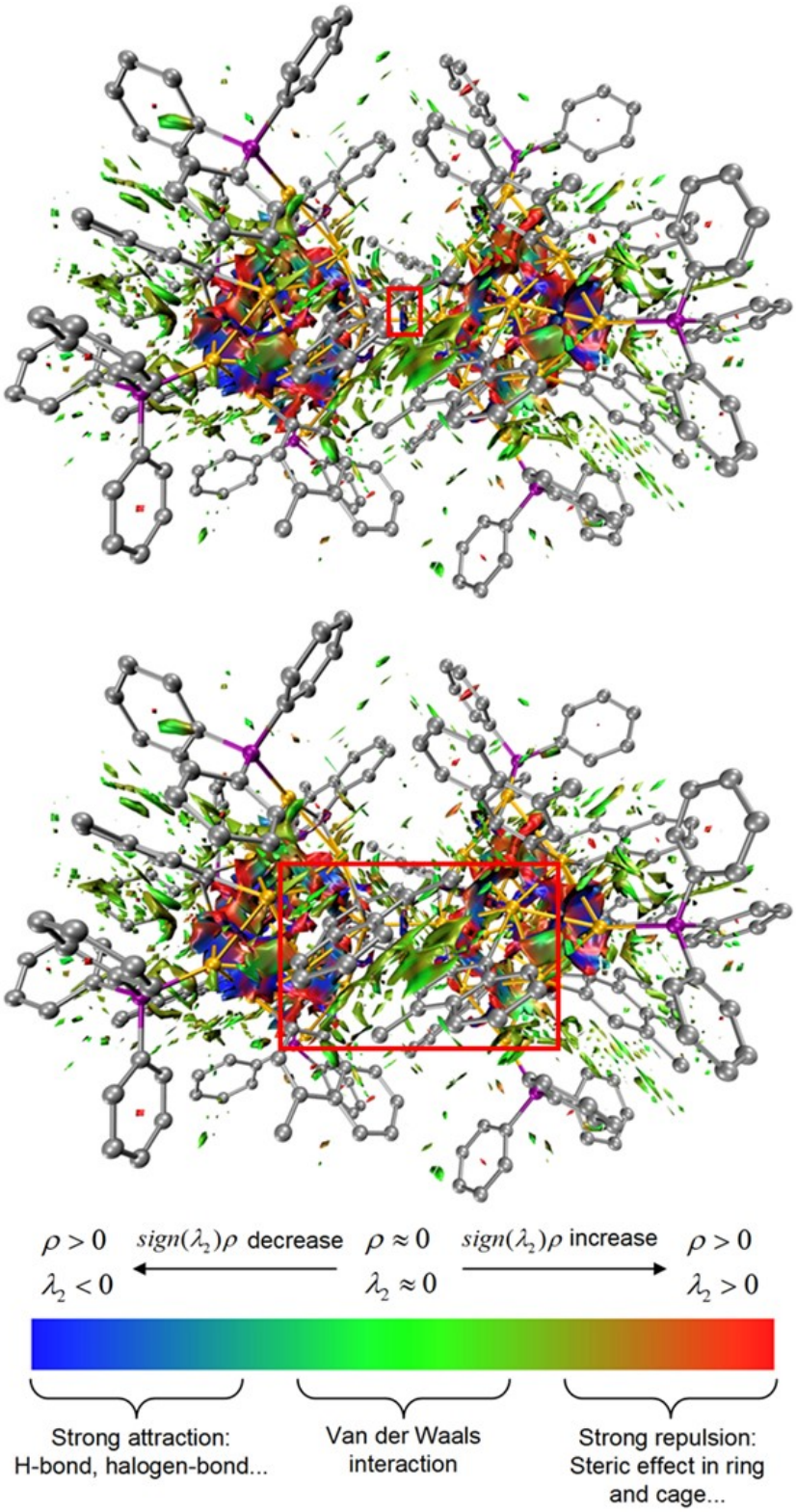

Fig. S15 Noncovalent interaction (NCI) map of **2c**. Isosurfaces of RDG = 0.5 are colored by sign(λ_2)ρ according to the color bar.[12]

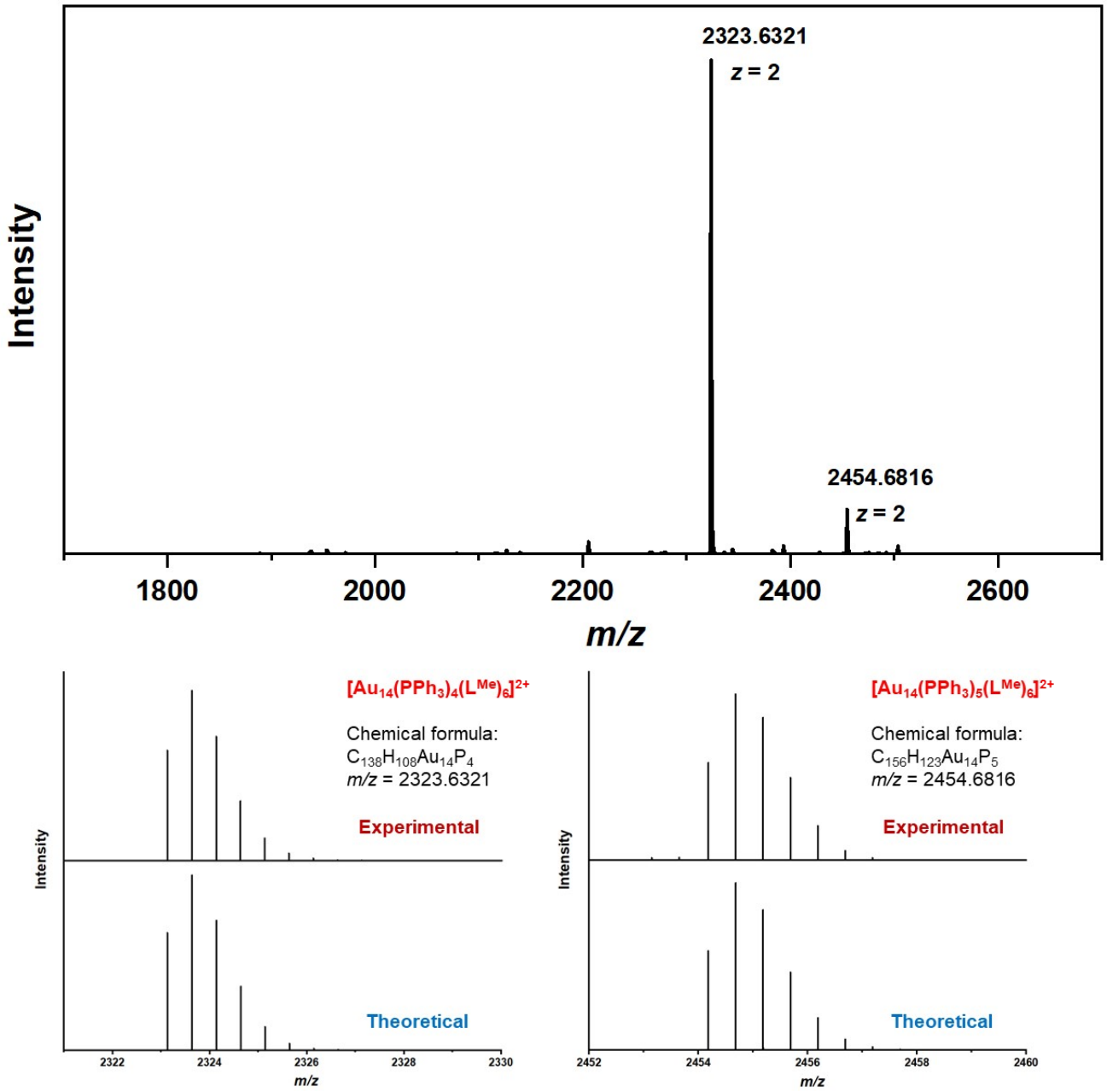

Fig. S16 High resolution ESI-MS spectra of complex **2c** in 1,2-dichloroethane.

Calcd. for $C_{138}H_{108}Au_{14}P_4$ 2323.1360 ($[Au_{14}(PPh_3)_4(L^{Me})_6]^{2+}$), found 2323.6321;

Calcd. for $C_{156}H_{123}Au_{14}P_5$ 2454.1815 ($[Au_{14}(PPh_3)_5(L^{Me})_6]^{2+}$), found 2454.6816.

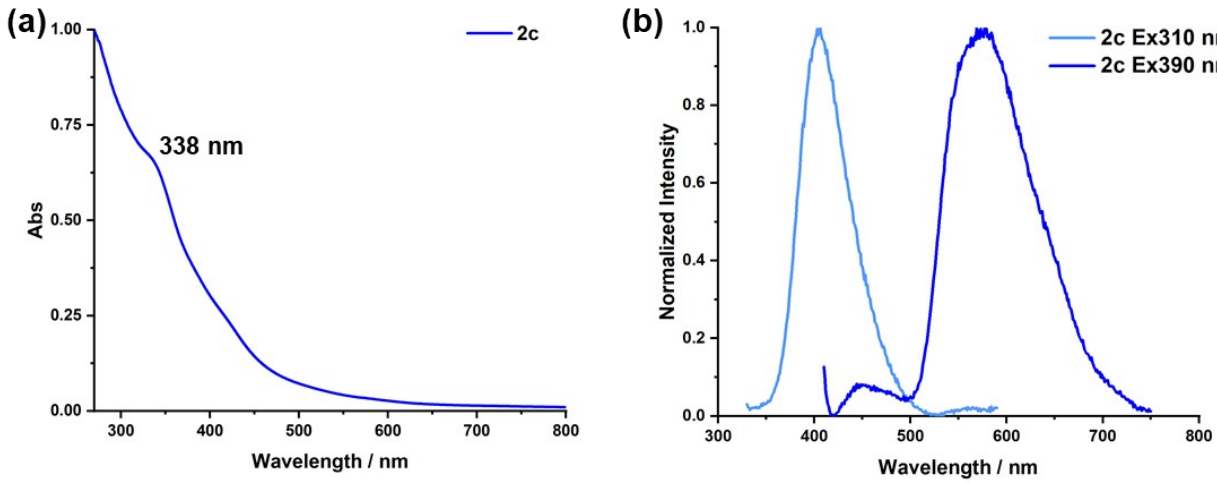

Fig. S17 UV-vis (a) and emission (b) spectra of complex **2c** in 1,2-dichloroethane.

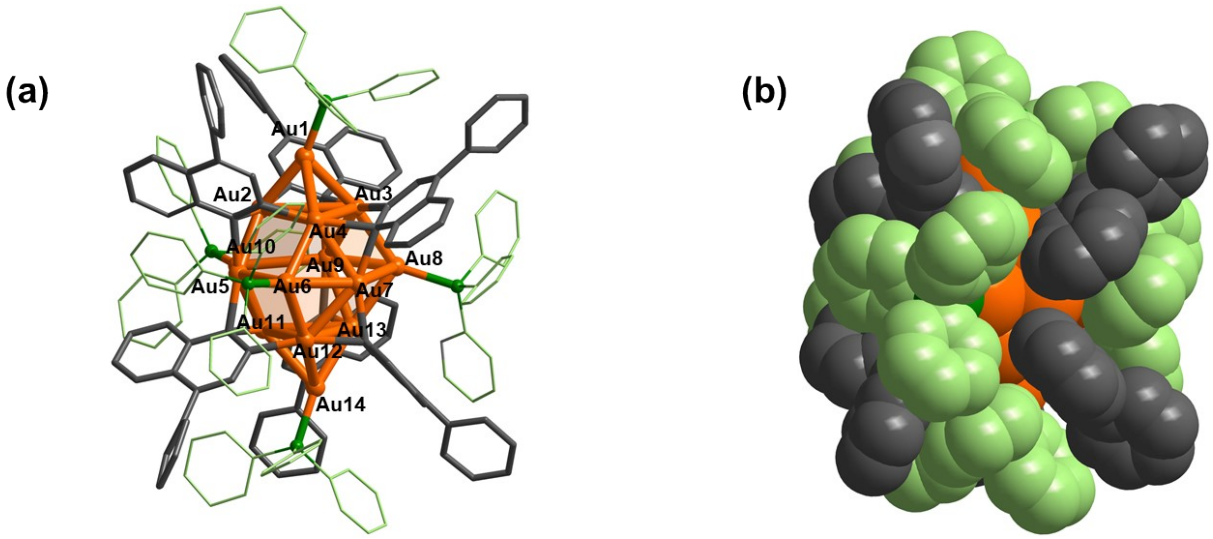

Fig. S18 (a) Crystal structure of complex **2d**. Hydrogen atoms, peripheral NTf_2^- counterions are omitted for clarity. Color coding: Au, orange; C, gray; P, green. Selected bond lengths (Å): Au1-Au2 2.6129(9); Au1-Au3 2.8055(11); Au1-Au4 2.9070(11); Au2-Au3 3.0413(3); Au2-Au4 2.7033(3); Au2-Au5 2.7141(3); Au2-Au10 2.7385(3); Au3-Au4 3.4271(9); Au3-Au8 2.5956(17); Au3-Au9 2.7469(7); Au4-Au6 2.7397(9); Au4-Au7 2.7234(8); Au5-Au10 2.8255(8); Au5-Au6 3.1463(9); Au5-Au11 2.8424(8); Au6-Au7 2.9653(10); Au6-Au12 2.7019(9); Au7-Au8 3.245(2); Au7-Au12 2.7832(8); Au8-Au9 2.867(5); Au8-Au13 2.696(3); Au9-Au10 3.2172(10); Au9-Au13 2.8777(8); Au10-Au11 2.6538(8); Au11-Au12 3.2067(8); Au11-Au13 3.1859(9); Au11-Au14 2.8636(9); Au12-Au13 3.4410(8); Au12-Au14 2.8529(9); Au13-Au14 2.6412(8). (b) Space-filling model of **2d**.

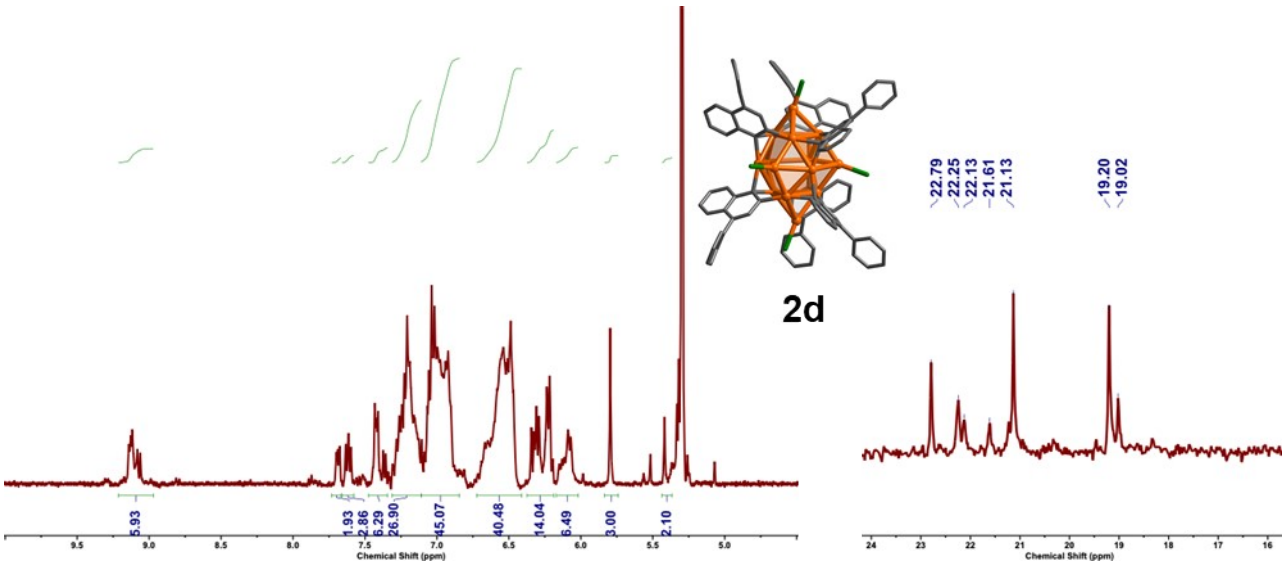

Fig. S19 ^{1}H and ^{31}P NMR spectra of complex **2d** in CD_2Cl_2. For low symmetry **2d** cluster, we have trouble assigning its NMR signals, but the broad range of peaks in ^{1}H NMR and low chemical shifts in ^{31}P NMR prove the integrity of **2d** assembly.

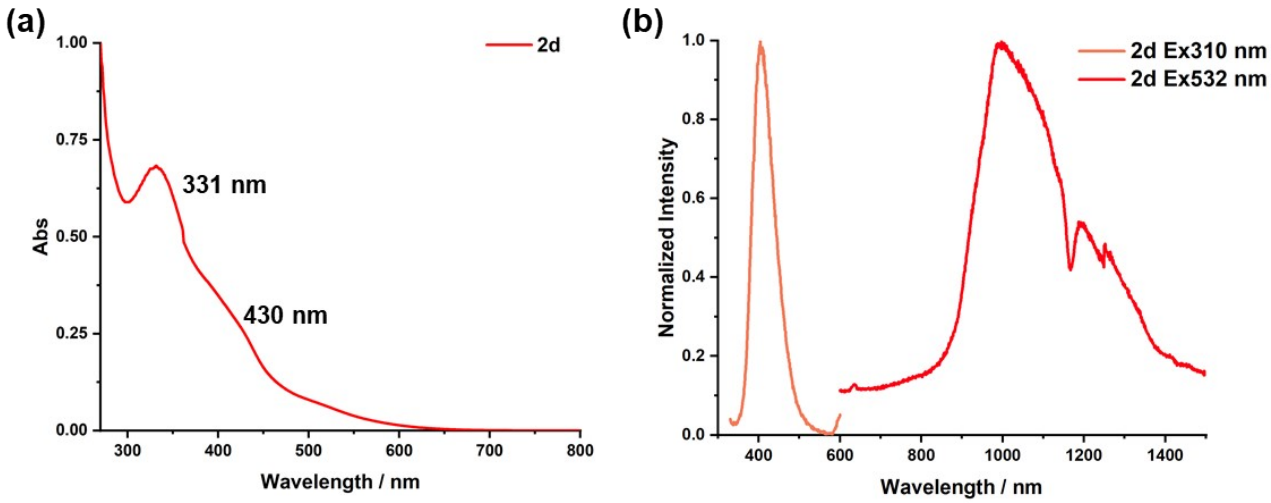

Fig. S20 UV-vis (a) and emission (b) spectra of complex **2d** in 1,2-dichloroethane. **2d** exhibits a unique near-infrared luminescence.

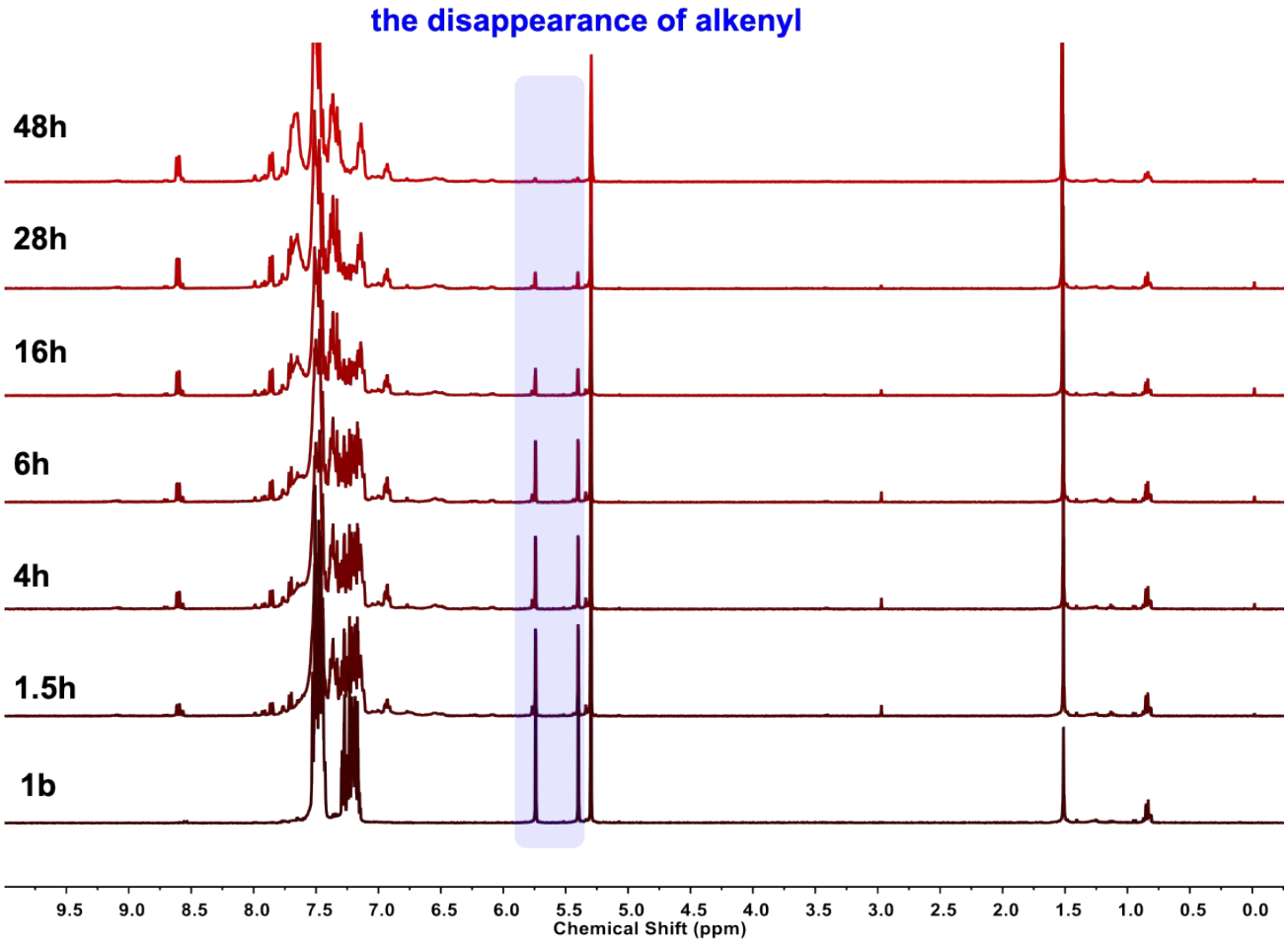

Fig. S21 ^{1}H NMR spectrum of the reaction process monitoring for **2b** to **2d** in CD_2Cl_2.

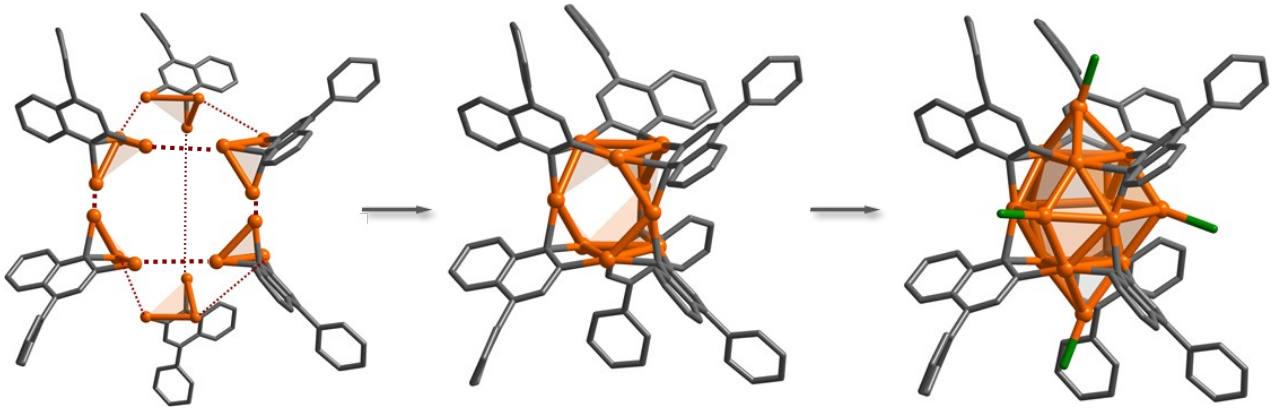

Fig. S22 The assembly pattern of cluster **2d**.

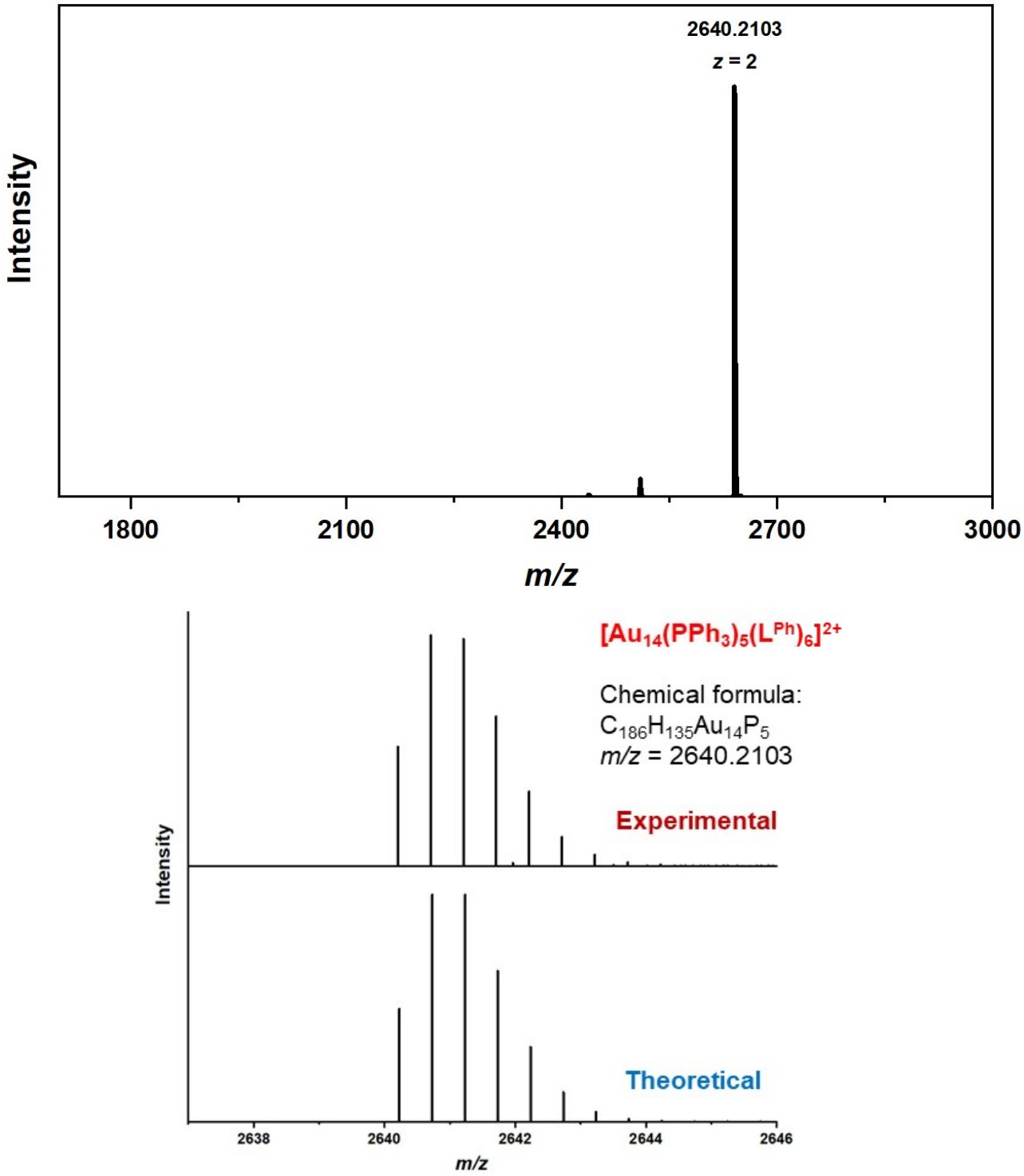

Fig. S23 High resolution ESI-MS spectra of complex **2d** in 1,2-dichloroethane. Calcd. for $C_{186}H_{135}Au_{14}P_5$ 2640.2279 ($[Au_{14}(PPh_3)_5(L^{Ph})_6]^{2+}$), found 2640.2103.

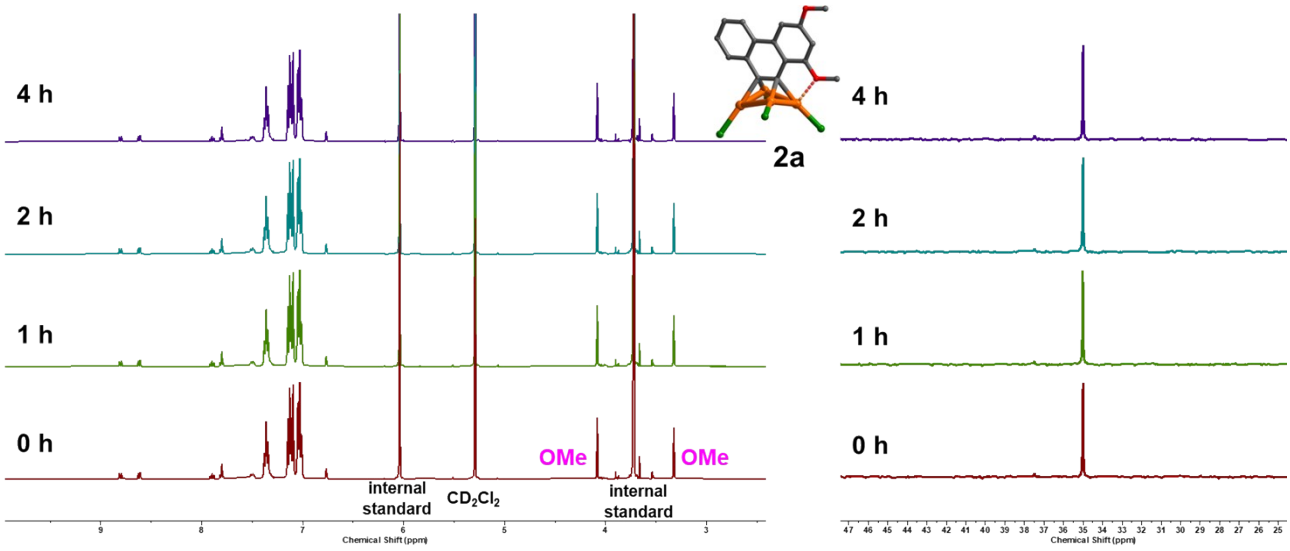

Fig. S24 The stability test of catalyst **2a** with 1,3,5-trimethoxybenzene as internal standard in CD_2Cl_2.

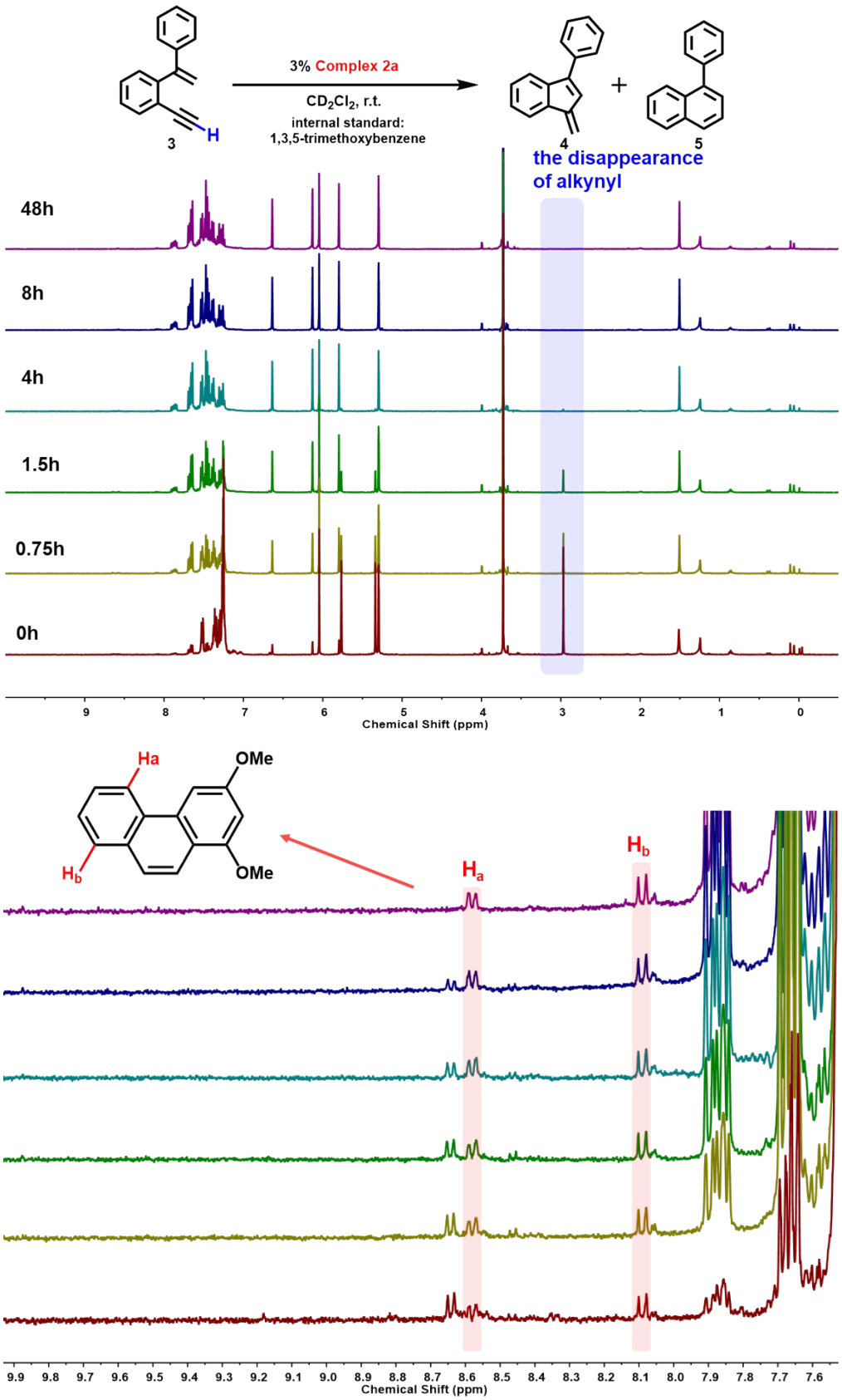

Fig. S25 (top) ^{1}H NMR spectrum of the reaction process monitoring of **2a** catalyzed cyclization of **3**. NMR data of 4 and 5 were consistent with that reported in literature.[13] (down) ^{1}H NMR expanded spectrum of the characteristic signals of **2a**.

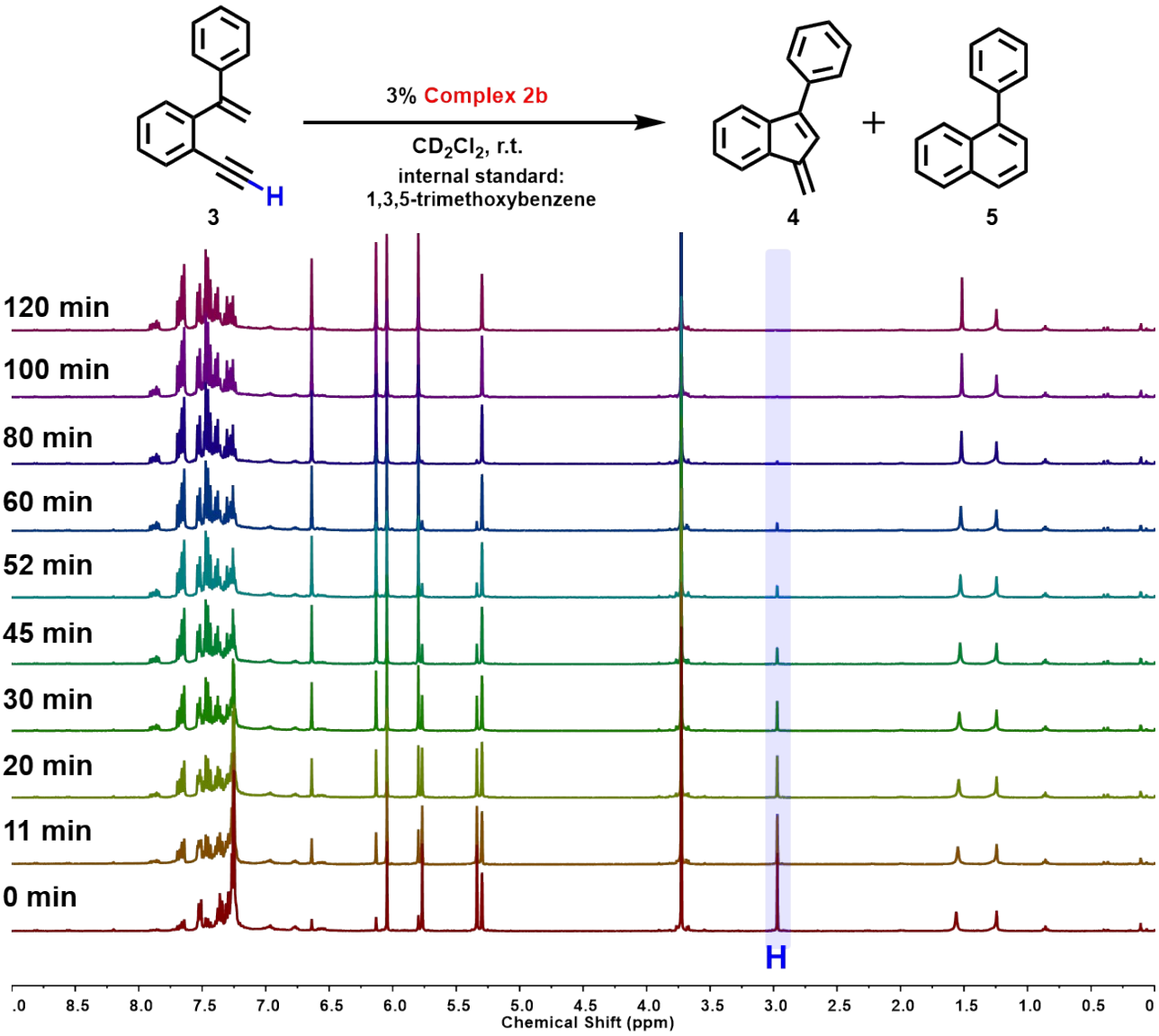

Fig. S26 ^{1}H NMR spectrum of the reaction process monitoring for the entire catalytic procedure of catalyst **2b**.

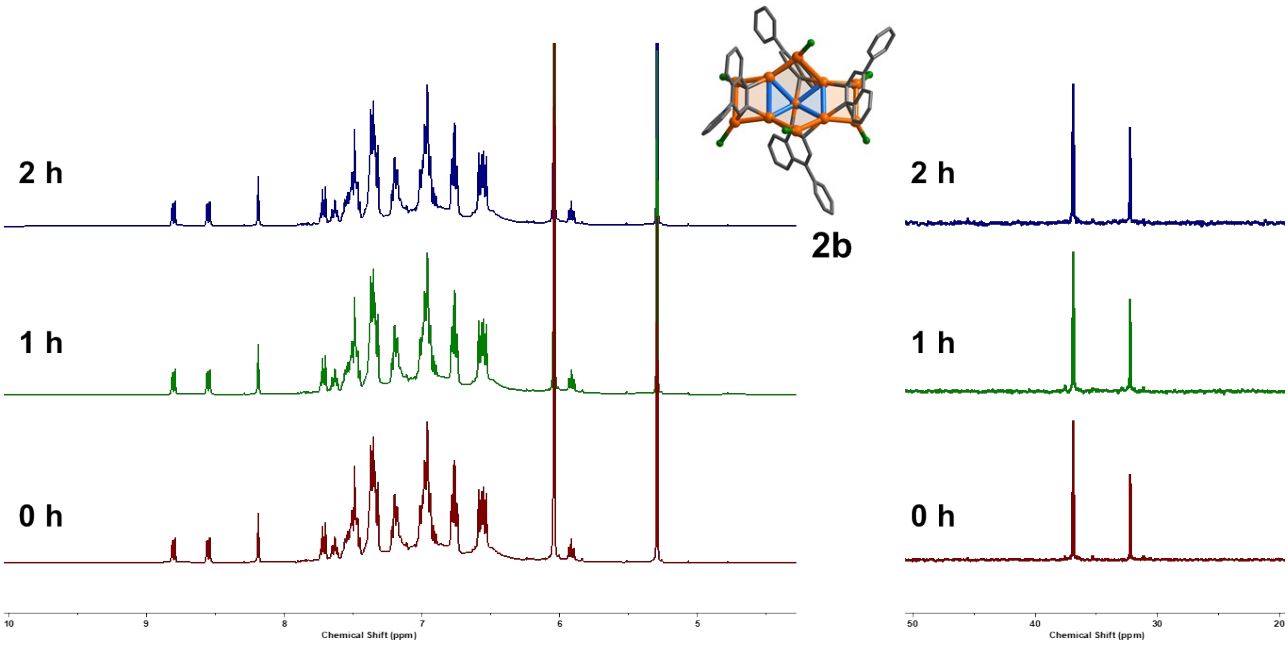

Fig. S27 The stability test of catalyst **2b** with 1,3,5-trimethoxybenzene as internal standard in CD_2Cl_2.

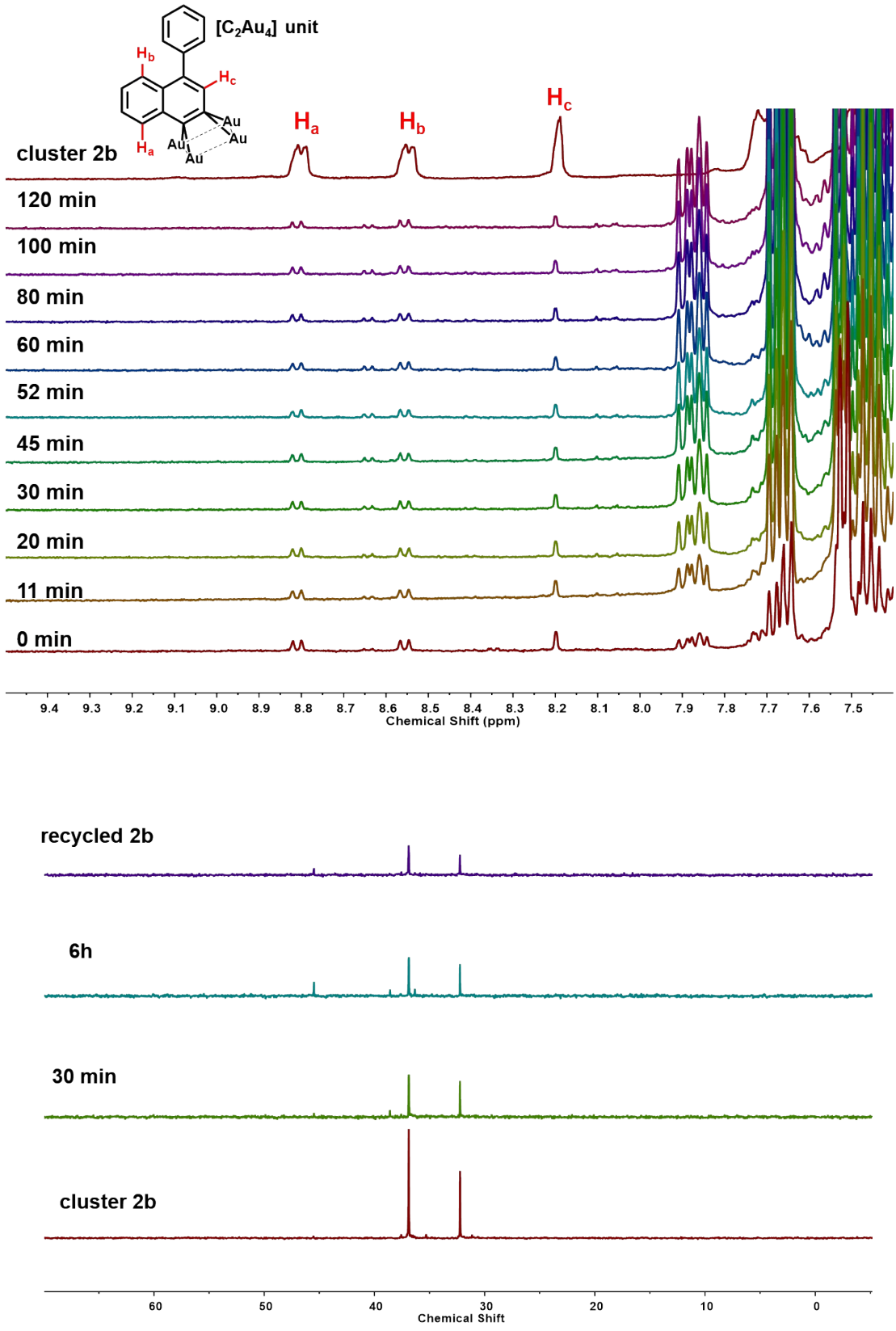

Fig. S28 (top) Partial enlarged ^{1}H NMR spectrum of characteristic peaks of complex **2b** during the catalytic reaction in CD_2Cl_2. (down) ^{31}P NMR spectrum of catalyst **2b**. The characteristic peak of **2b** had no obvious change, but a new peak of $[Au(PPh_3)_2]^+$ with low concentration appeared at 45.5 ppm. It was indicated that $[Au(PPh_3)]^+$ was involved in the reaction process and a small portion decomposed into $[Au(PPh_3)_2]^+$.

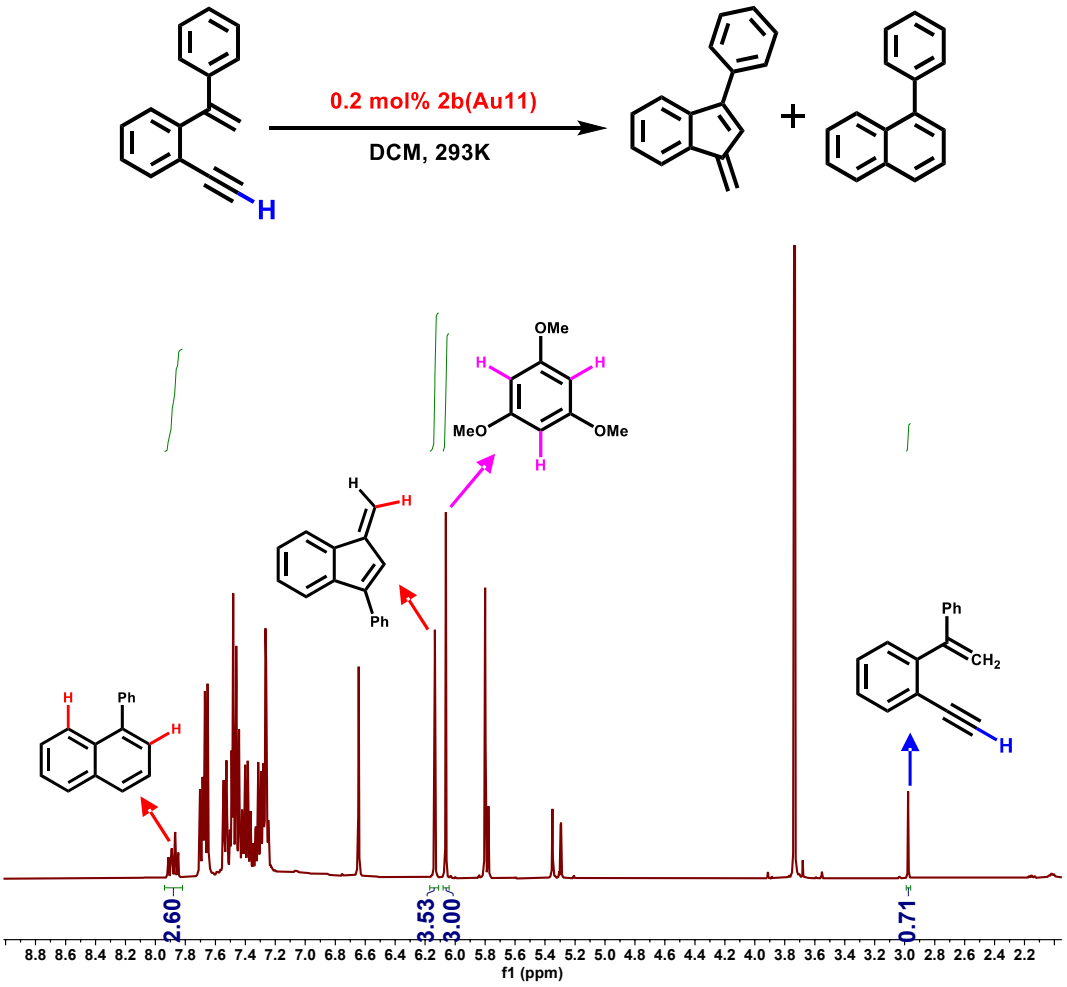

Fig. S29 The TON of the reaction with clusters **2b**. In a 5 mL glass bottle, enyne substrate **3** (18.5 mg, 0.09 mmol), **2b** (1.0 mg, $1.8*10^{-4}$ mmol) were combined in CH_2Cl_2 (0.5 mL) at 293K. After the reactions were completed, we added 1,3,5-trimethoxybenzene (0.015 mmol, 2.5 mg) as internal standard and analyze the reaction systems by ^1H NMR spectra. The TON of **2b** is 403.

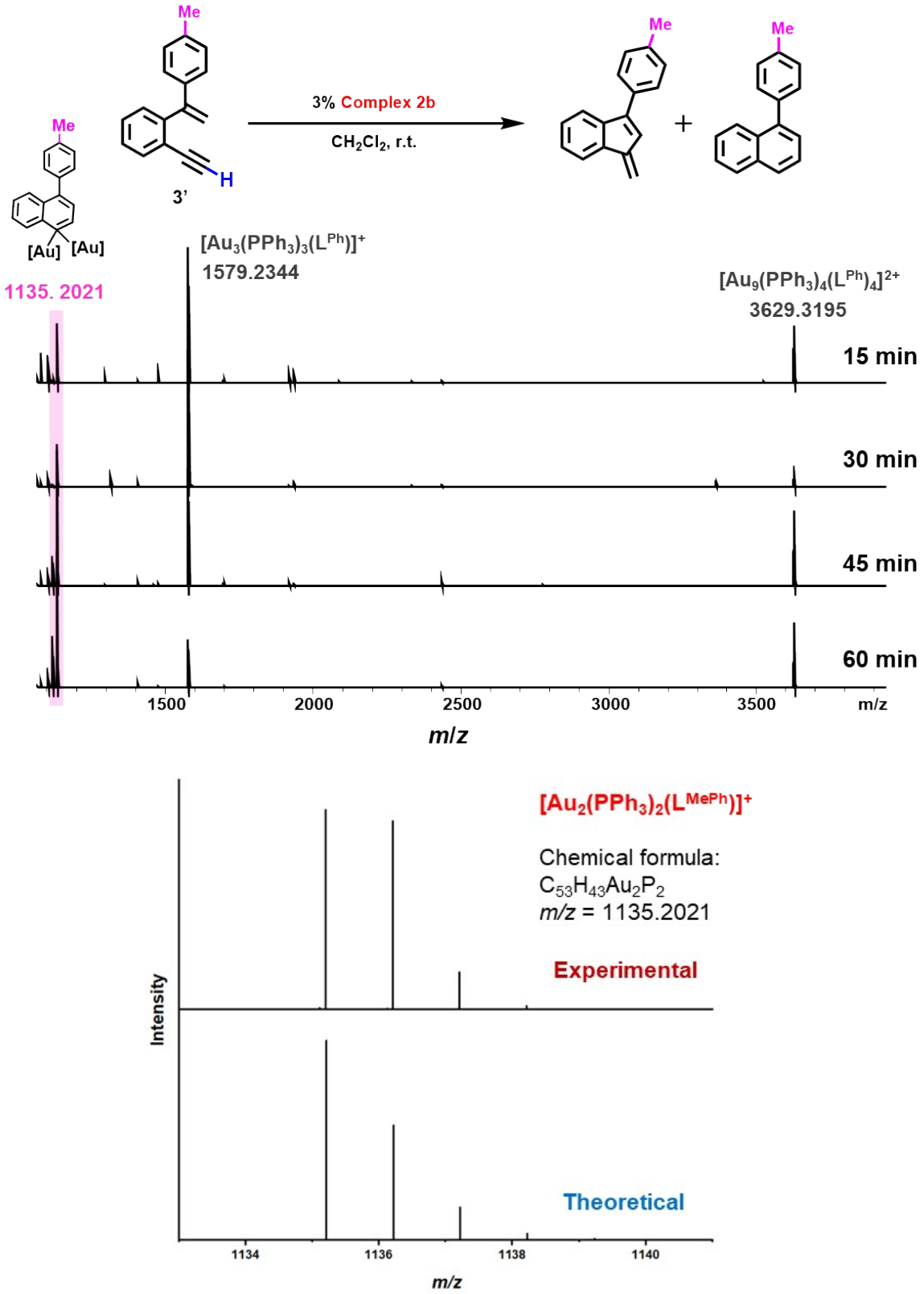

Fig. S30 ESI-MS spectrum of catalyst **2b** during the overcross catalytic reaction in CH_2Cl_2. Due to the inherent nature of **2b**, it was difficult to detect the completed molecular ion peak, and only some fragment peaks could be observed. Specially, we found symbolic *gem*-diaurated species (*m/z* values of 1135.2021) for $[Au(PPh_3)]^+$ catalytic system (calcd. for $C_{53}H_{43}Au_2P_2$ 1135.2166 ($[Au_2(PPh_3)_2(L^{MePh})]^+$).

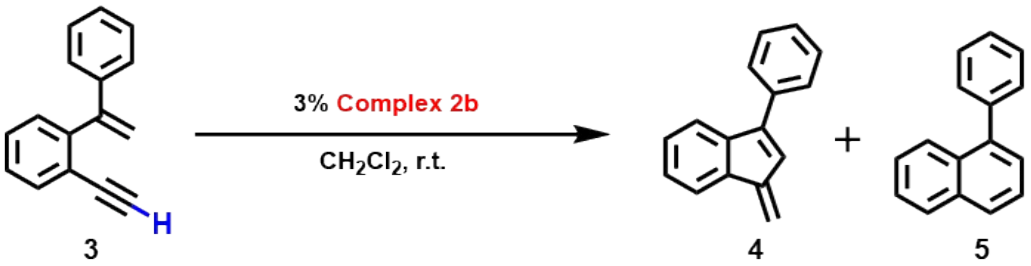

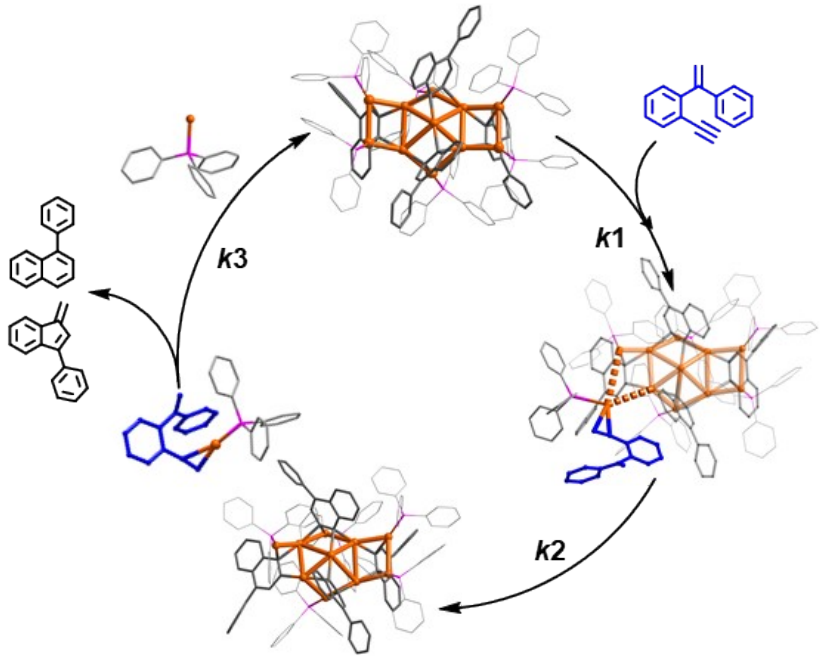

According to the well-established mechanism,

a rate law of the form: rate = $-k(k1,k2,k3)[Au_{11}][3] = -K_{obs}[3]$ can be derived.

Fig. S31 Proposed mechanism for the cyclization reaction catalyzed by **2b** and the kinetic analyses of the reaction.

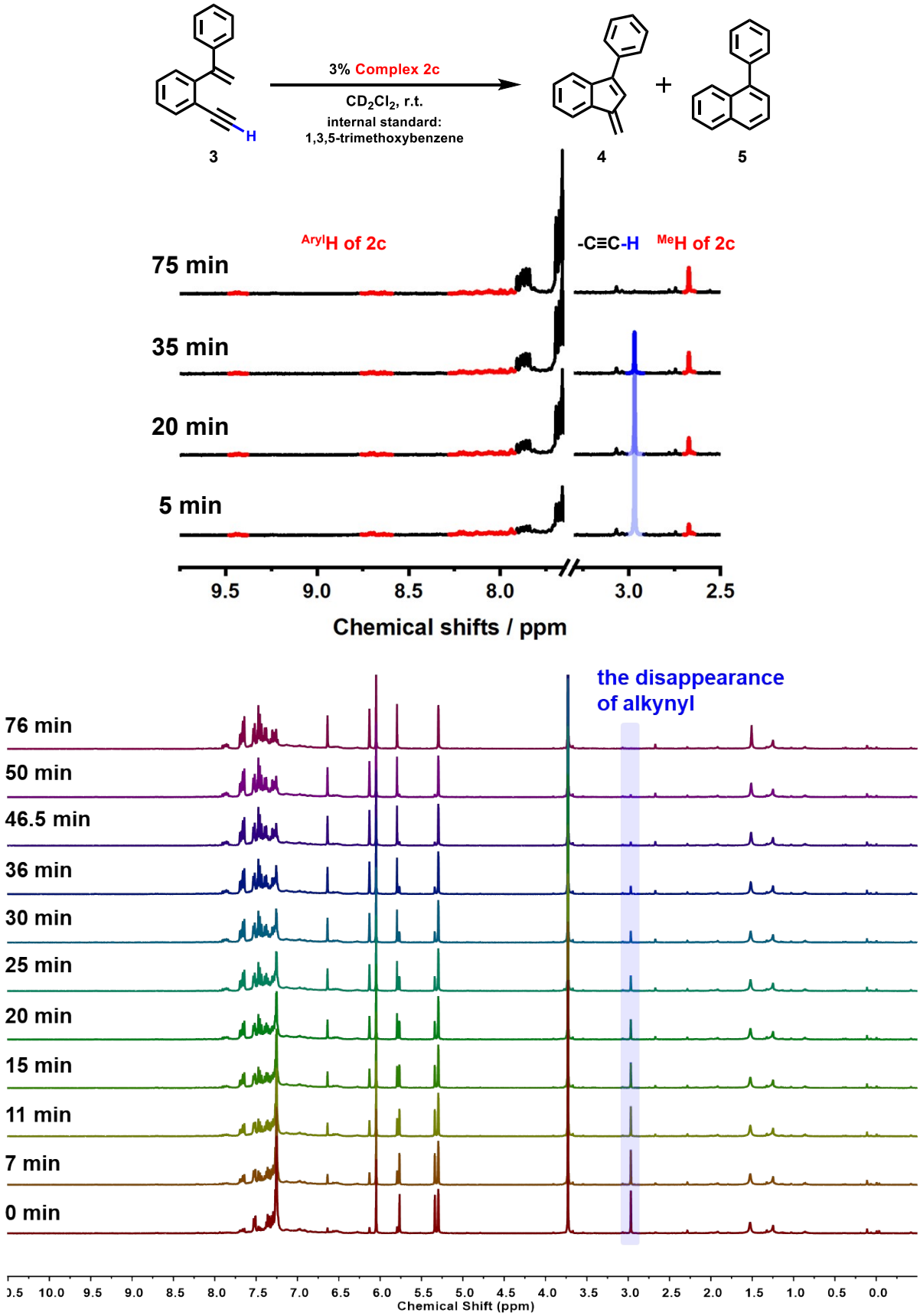

Fig. S32 (top) ^{1}H NMR monitoring of the catalytic procedure of catalyst **2c**. Red lines represent the cluster structure peak, and blue lines represent the decline of the alkyne peak. (down) ^{1}H NMR spectrum of the entire catalytic procedure.

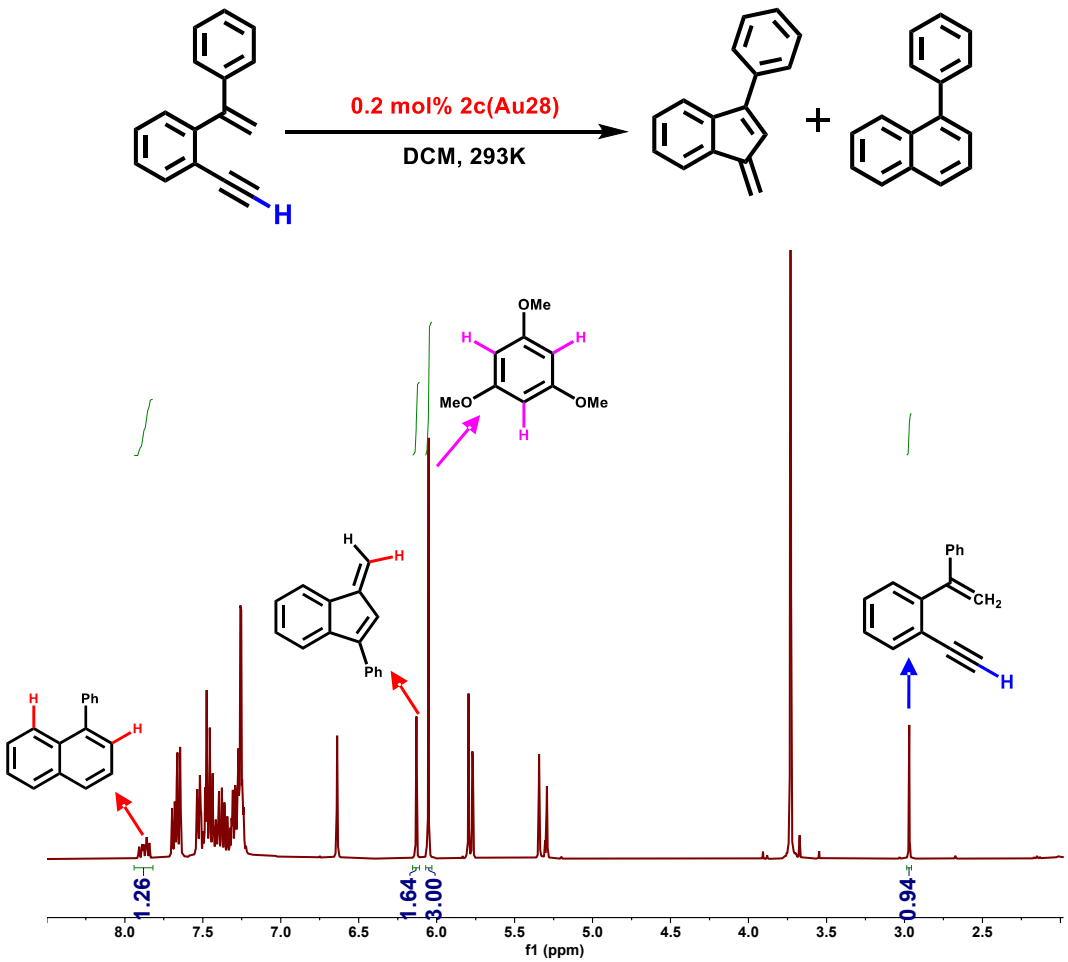

Fig. S33 The TON of the reaction with clusters **2c**. In a 5 mL glass bottle, enyne substrate **3** (10.3 mg, 0.05 mmol), **2c** (1.0 mg, $1*10^{-4}$ mmol) were combined in CH_2Cl_2 (0.3 mL) at 293K. After the reactions were completed, we added 1,3,5-trimethoxybenzene (0.015 mmol, 2.5 mg) as internal standard and analyze the reaction systems by ^1H NMR spectra. The TON of **2c** is 341.

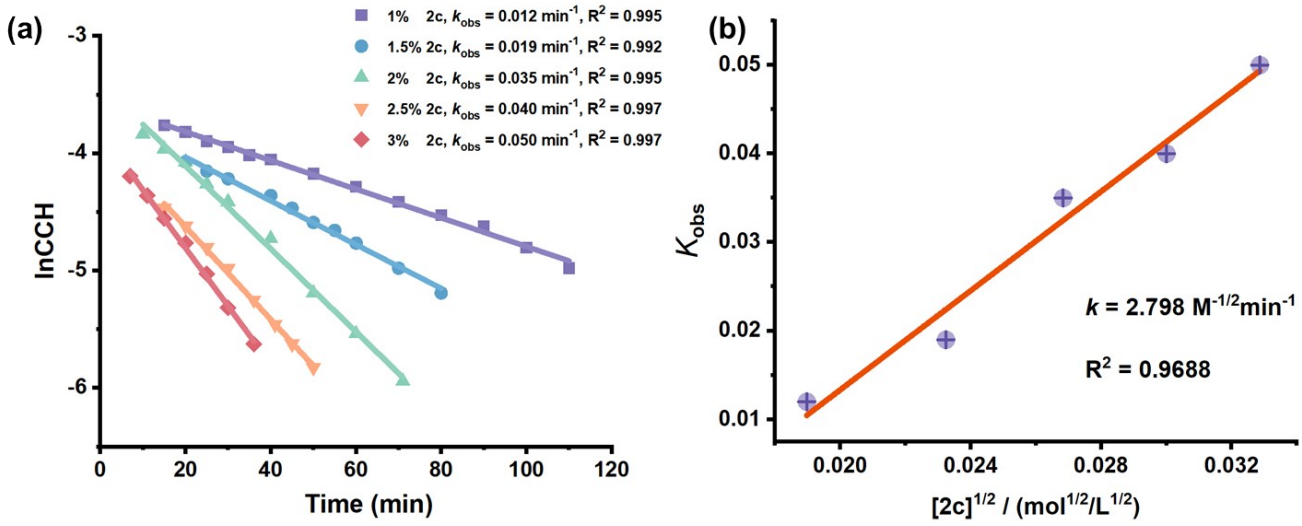

Fig. S34 (a) Pseudo-first-order kinetic curves of **2c** catalyzed reactions. (b) Kinetic curves of **2c** depended on the catalyst concentration.

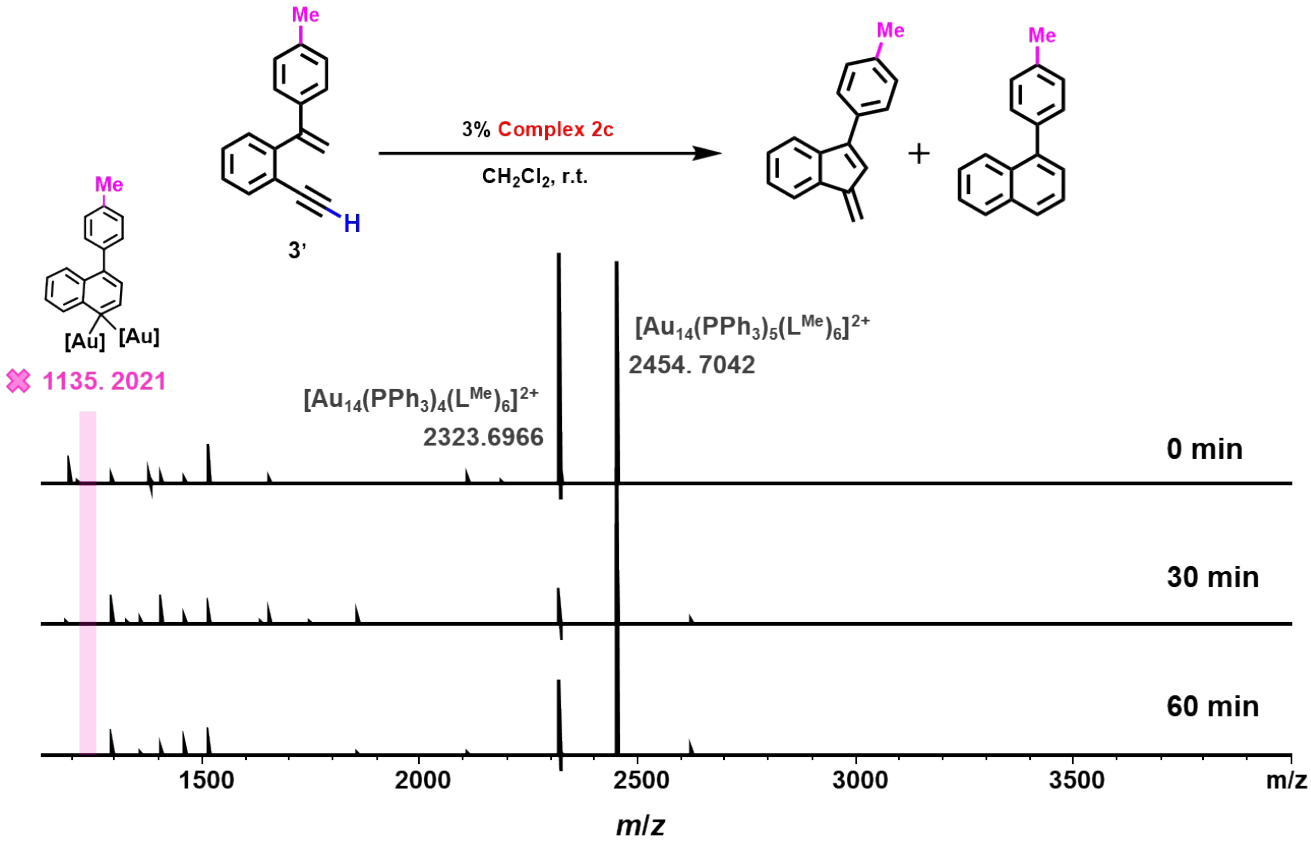

Fig. S35 ESI-MS spectrum of catalyst **2c** during the overcross catalytic reaction in CH_2Cl_2. The characteristic peak of **2c** had no obvious change and *gem*-diaurated species for $[Au(PPh_3)]^+$ catalytic system were not found.

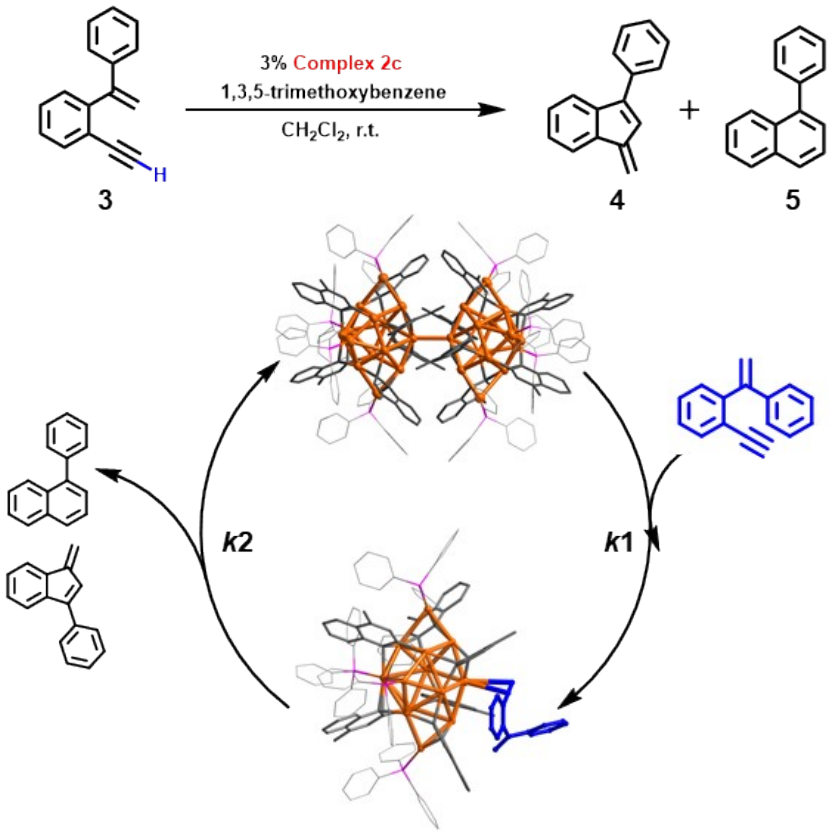

According to the well-established mechanism,

a rate law of the form: rate = $-k(k1,k2)[^{Me}Au_{14}][3] = -K_{obs}[3]$ can be derived.

$$[Au_{28}] \rightleftharpoons 2[^{Me}Au_{14}],\ K_{eq} = \frac{[^{Me}Au_{14}]^2}{[Au_{28}]},\ [^{Me}Au_{14}] = [K_{eq}[Au_{28}]]^{1/2}$$

$$\text{Thus, rate} = -k(k1,k2,K_{eq})[Au_{28}]^{1/2}[3]$$

Fig. S36 Proposed mechanism for the cyclization reaction catalyzed by **2c** and the kinetic analyses of the reaction.

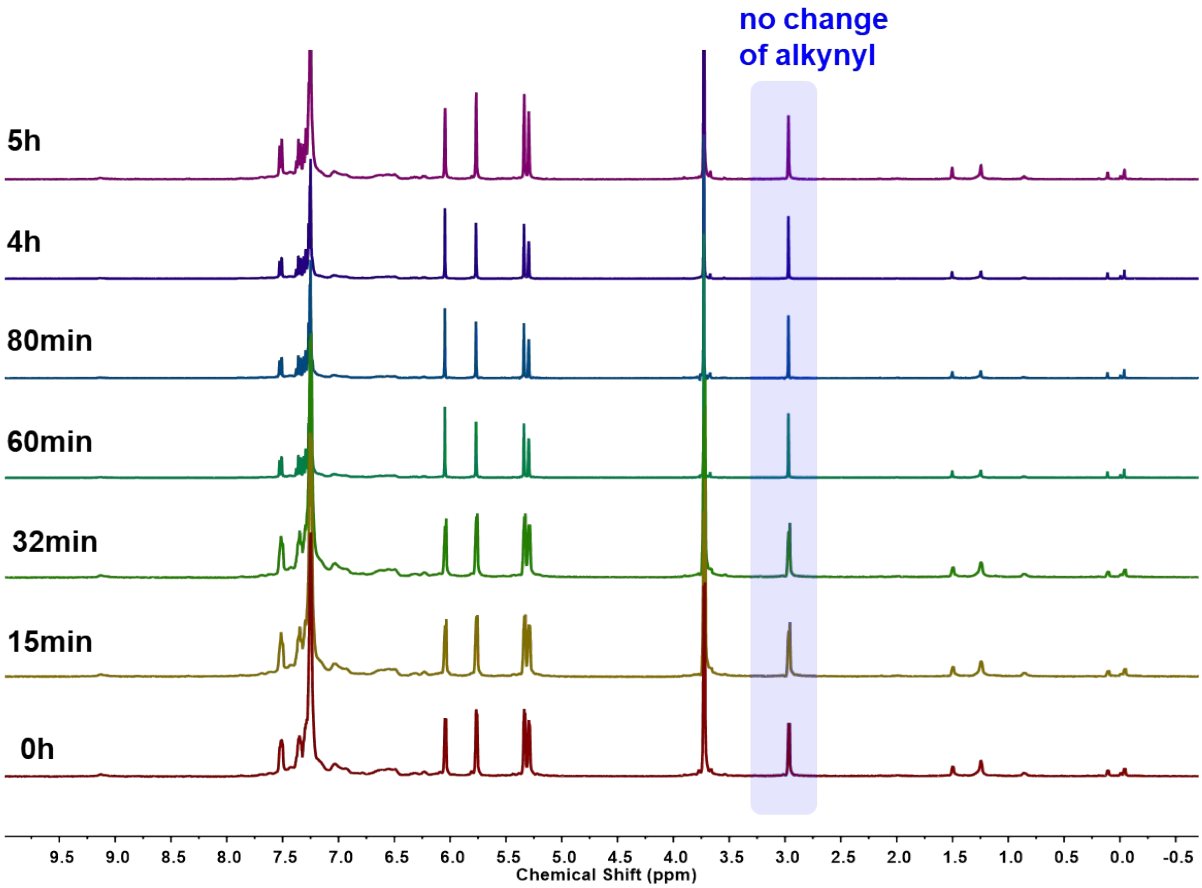

Fig. S37 ^{1}H NMR spectrum of the reaction process monitoring of **2d** catalyzed cyclization of **3**.

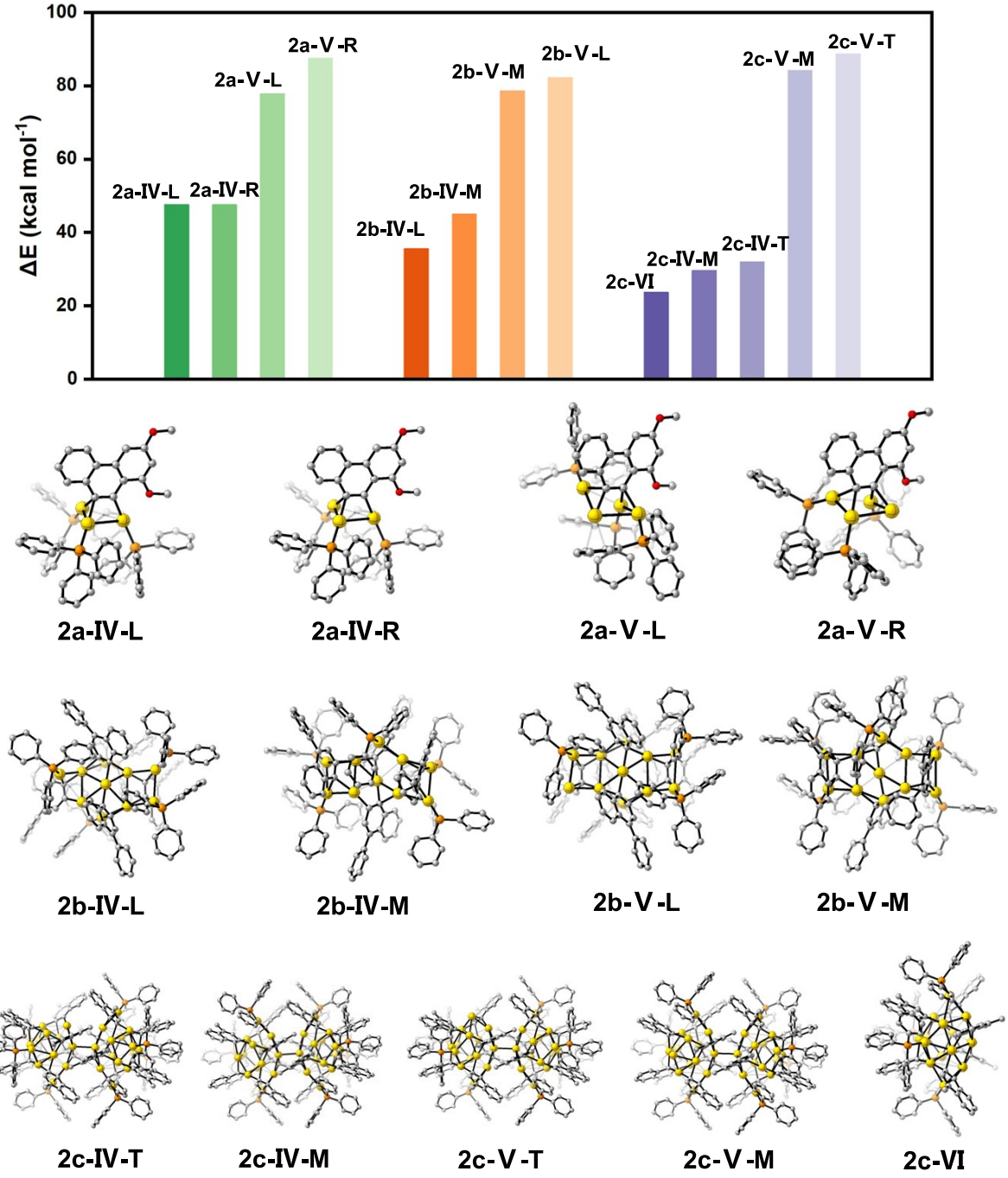

Fig. S38 DFT results for energies (kcal mol^{-1}) of the cluster stability. (top) Comparison of the energetics (ΔE) of different dissociation types of metal clusters **2a-2c**. (down) The structures of dissociation products, **IV** represents that clusters undergo the removal of $[Au(PPh_3)]^+$ fragment, **V** represents that clusters undergo synergistic coordination of the alkyne and dissociation of the PPh_3, and VI depicts the pathway for the dissociation of **2c** into two $^{Me}\mathbf{Au_{14}}$ units. There are two chemical non-equivalent Au sites in each structure: L, left; R, right; M, middle; T, top.

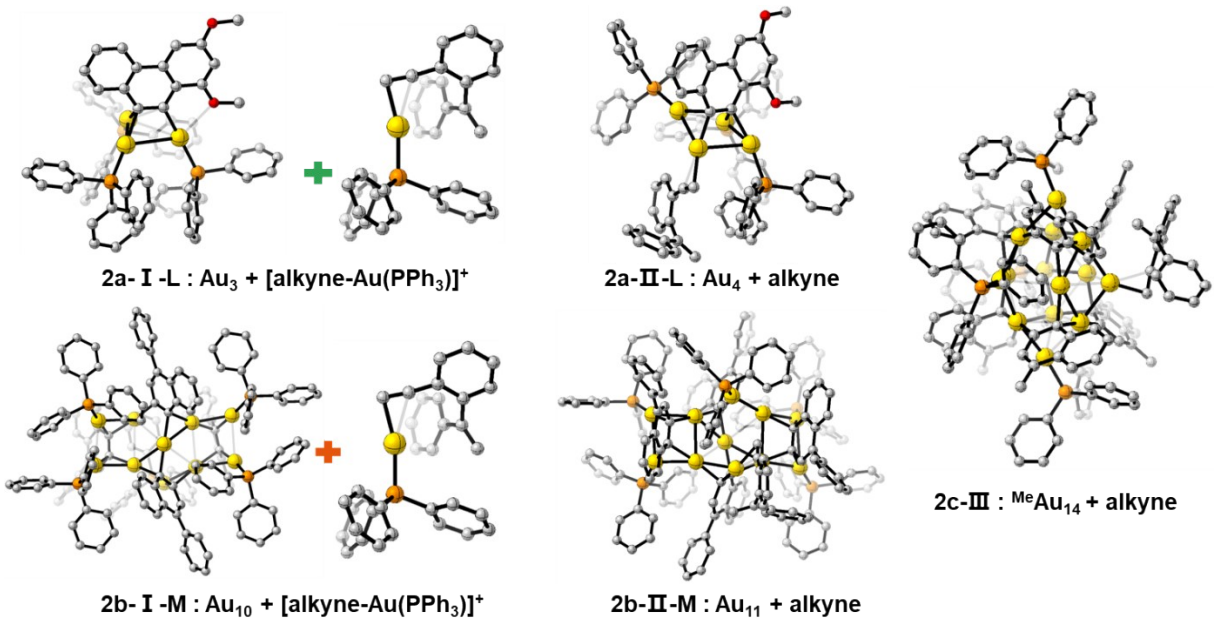

Fig. S39 Complementary structures of intermediates of clusters **2a-2c** in Figure 5 (L, left; R, right; M, middle).

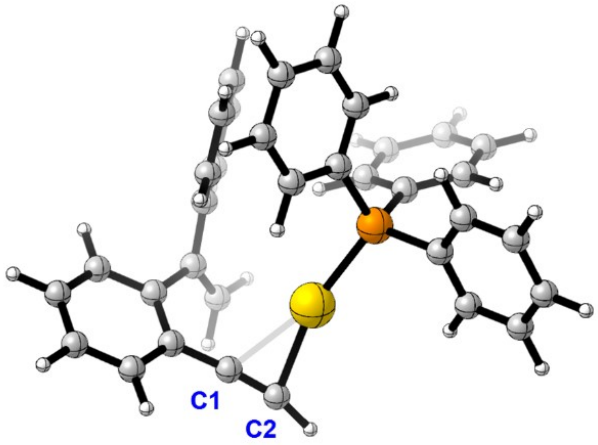

atomic charge	C1 (*5-exo-dig*)	C2 (*6-endo-dig*)
Hirshfeld	0.0152	-0.0609
Mulliken	0.177	-0.205
ADCH	-0.150	-0.409

Fig. S40 Atomic charge calculation for [alkyne-Au(PPh_3)]$^+$. The Hirshfeld, Mulliken and ADCH actomic charge are more positive for C1 than C2, which indicated C1 is more electrophilic than C2 and easily attacked by alkenyl group to give five-membered ring product.

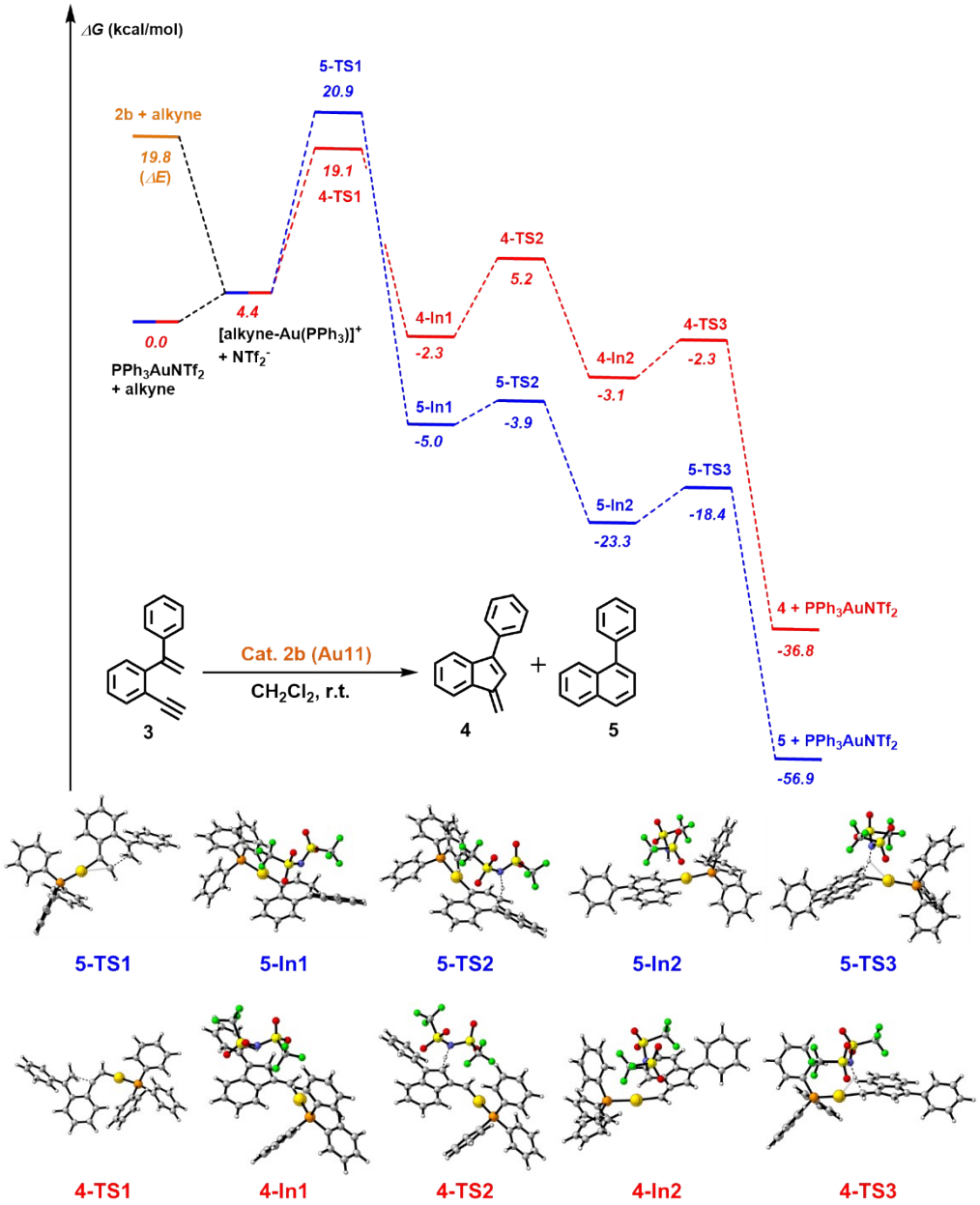

Fig. S41 Potential energy profile of single-point energies (for **2b** and $\mathbf{Au_{10}}$) combined with Gibbs free energy (for mononuclear species). Gibbs free energies and single point energies are in kcal mol^{-1}. Relative energies (kcal mol^{-1}): $\mathbf{PPh_3AuNTf_2}$ + $\mathbf{Au_{10}}$ + **alkyne** = 0, **2b** + **alkyne** = 19.8, $\mathbf{[alkyne\text{-}Au(PPh_3)]^+ + NTf_2^-}$ + $\mathbf{Au_{10}}$ = 4.4, **4-TS1** + $\mathbf{Au_{10}}$ = 19.1, **4-In1** + $\mathbf{Au_{10}}$ = -2.3, **4-TS2** + $\mathbf{Au_{10}}$ = 5.2, **4-In2** + $\mathbf{Au_{10}}$ = -3.1, **4-TS3** + $\mathbf{Au_{10}}$ = -2.3, **4** + $\mathbf{PPh_3AuNTf_2}$ + $\mathbf{Au_{10}}$ = -36.8. **5-TS1** + $\mathbf{Au_{10}}$ = 20.9, **5-In1** + $\mathbf{Au_{10}}$ = -5.0, **5-TS2** + $\mathbf{Au_{10}}$ = -3.9, **5-In2** + $\mathbf{Au_{10}}$ = -23.3, **5-TS3** + $\mathbf{Au_{10}}$ = -18.4, **5**+ $\mathbf{PPh_3AuNTf_2}$ + $\mathbf{Au_{10}}$ = -56.9.

Supplementary Spectrum.

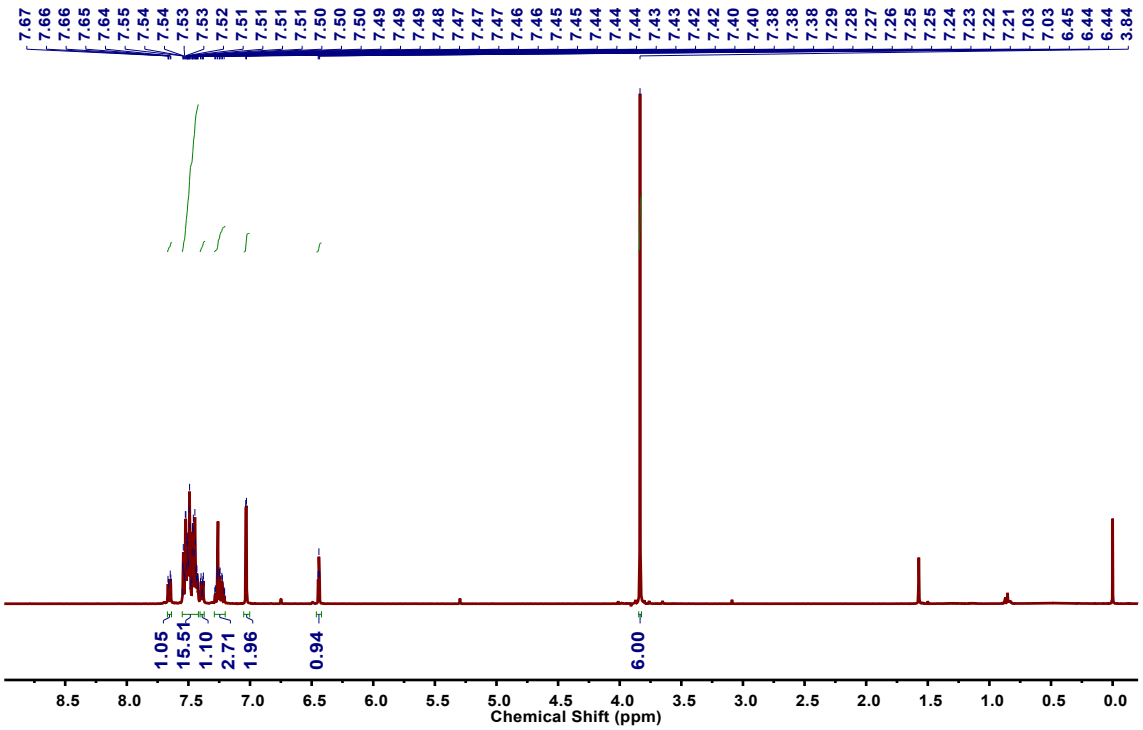

Fig. S42 ^{1}H NMR spectrum (400 MHz, $CDCl_3$, 298 K) of **1a**.

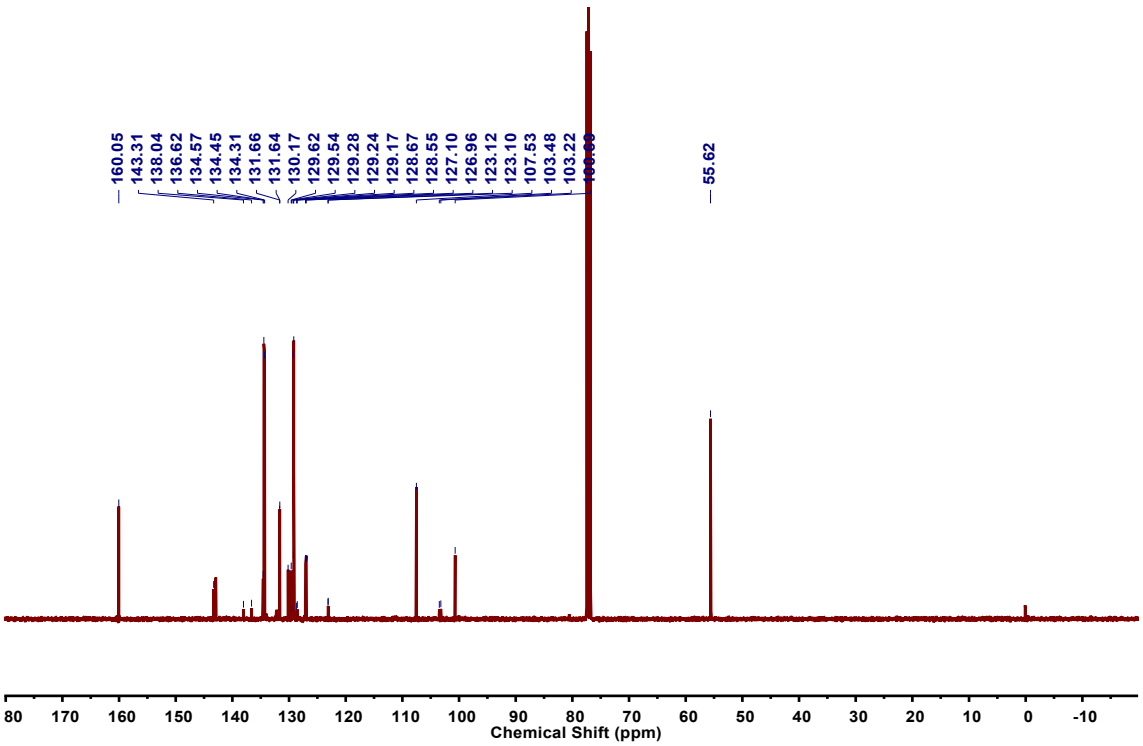

Fig. S43 ^{13}C NMR spectrum (100 MHz, $CDCl_3$, 298 K) of **1a**.

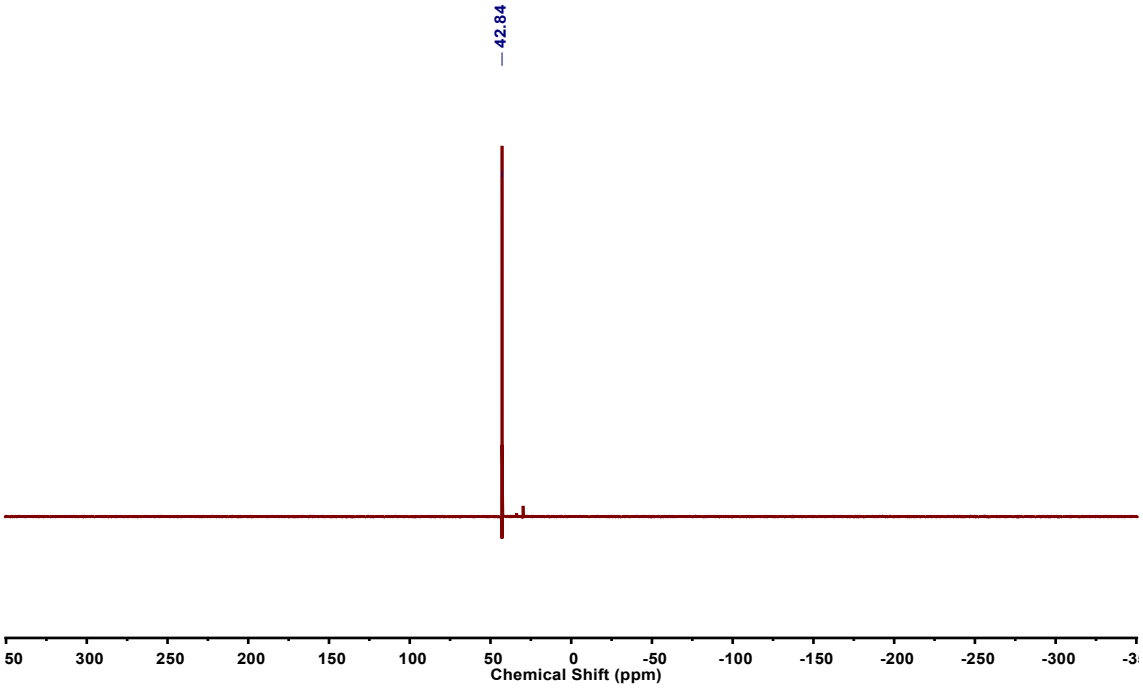

Fig. S44 ^{31}P NMR spectrum (162 MHz, $CDCl_3$, 298 K) of **1a**.

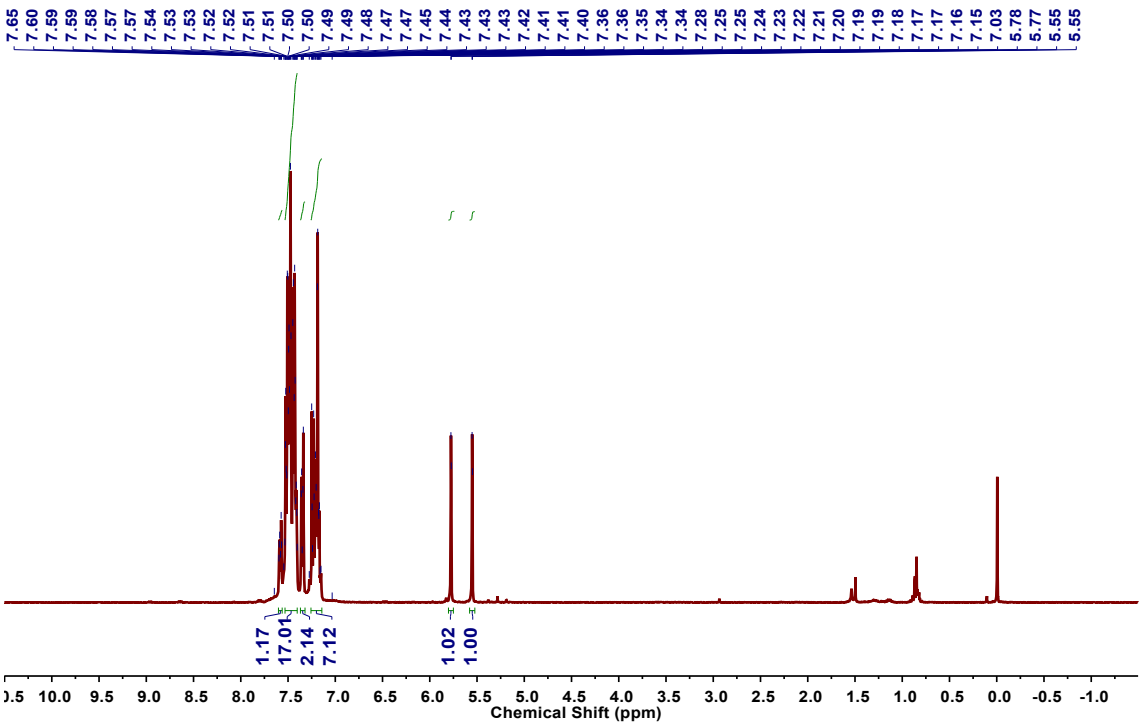

Fig. S45 ^{1}H NMR spectrum (400 MHz, $CDCl_3$, 298 K) of **1b**.

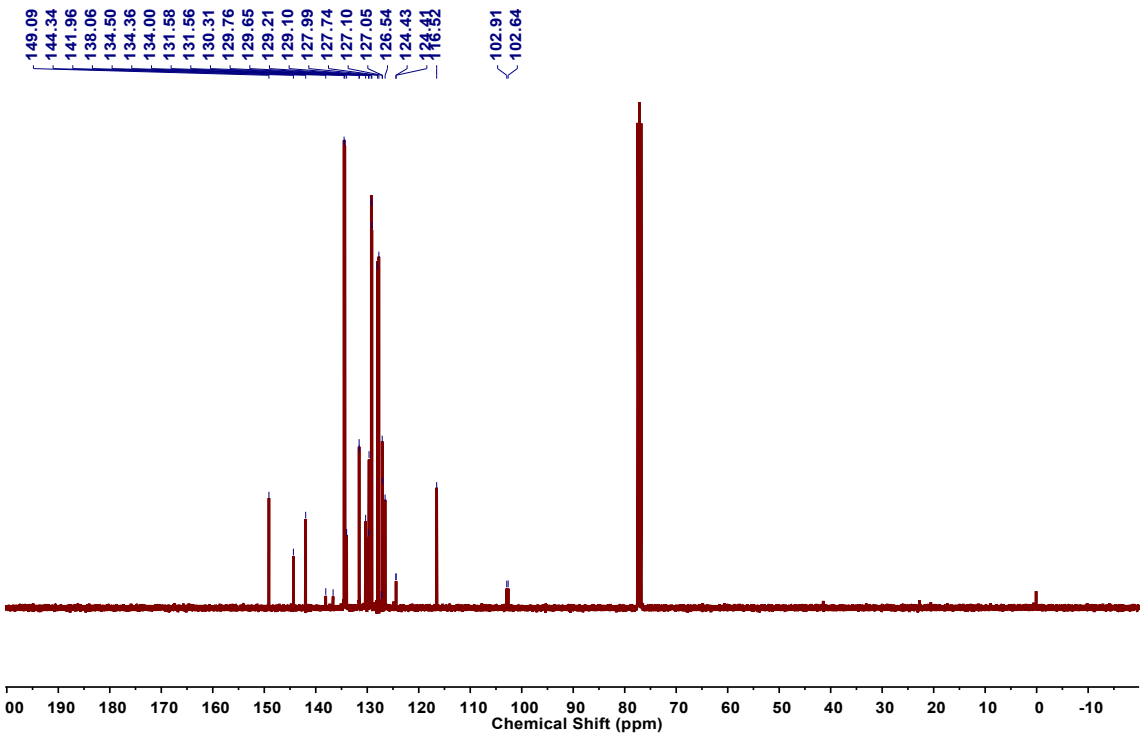

Fig. S46 ^{13}C NMR spectrum (100 MHz, $CDCl_3$, 298 K) of **1b**.

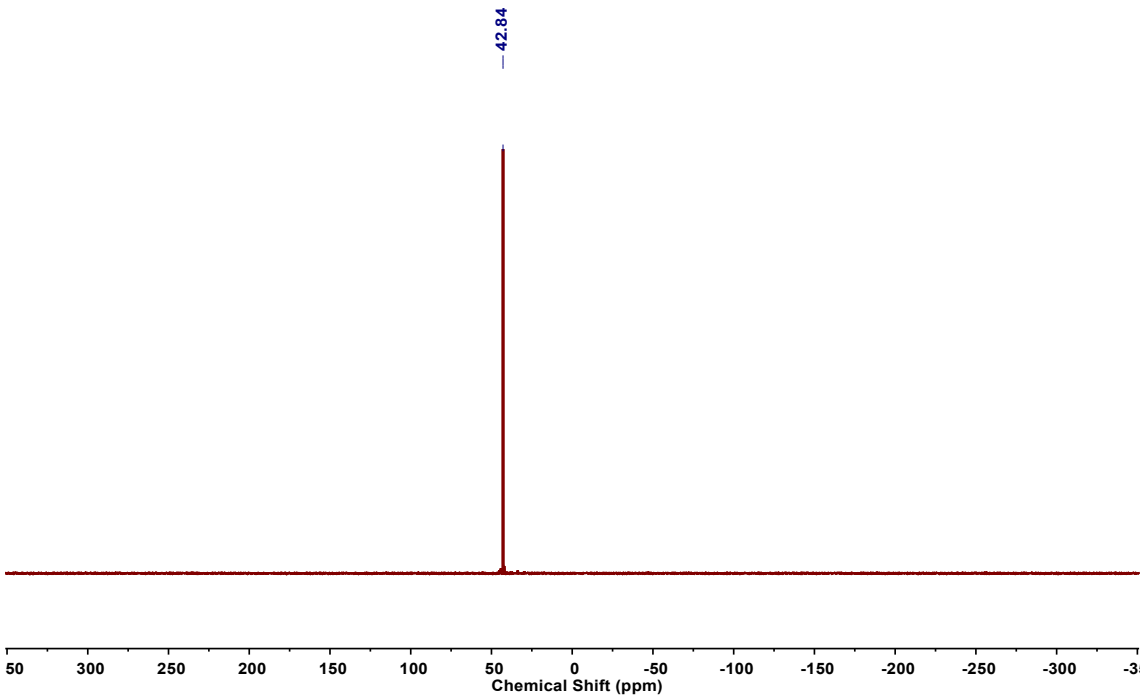

Fig. S47 ^{31}P NMR spectrum (162 MHz, $CDCl_3$, 298 K) of **1b**.

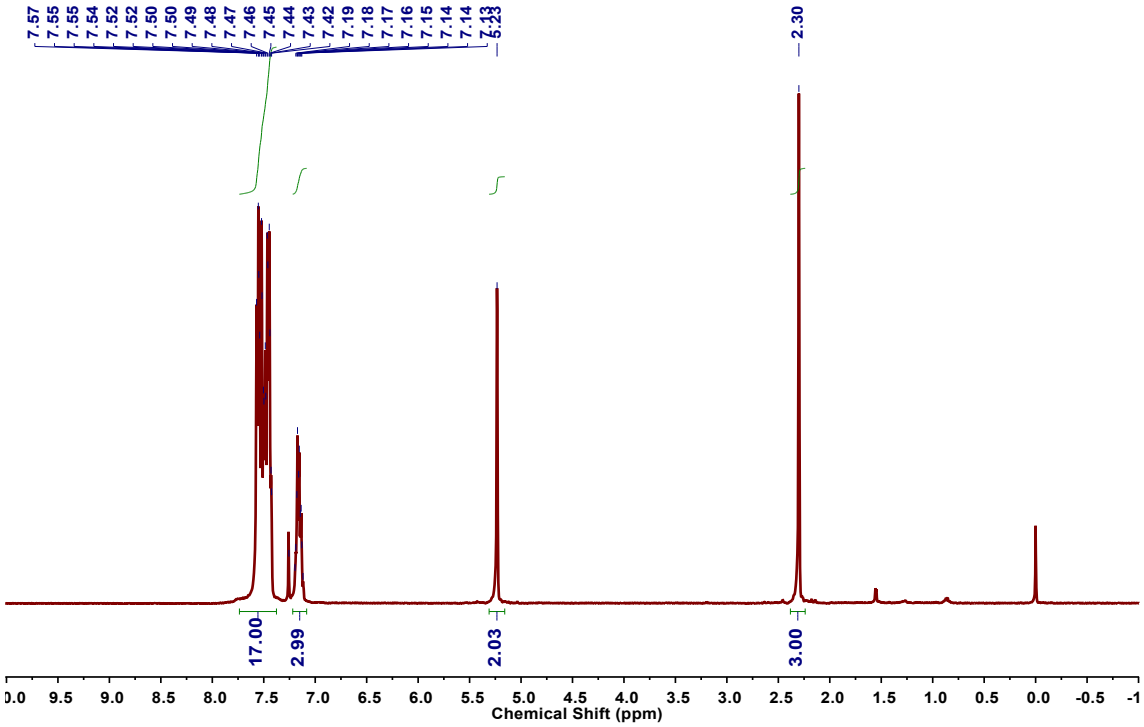

Fig. S48 ^{1}H NMR spectrum (400 MHz, $CDCl_3$, 298 K) of **1c**.

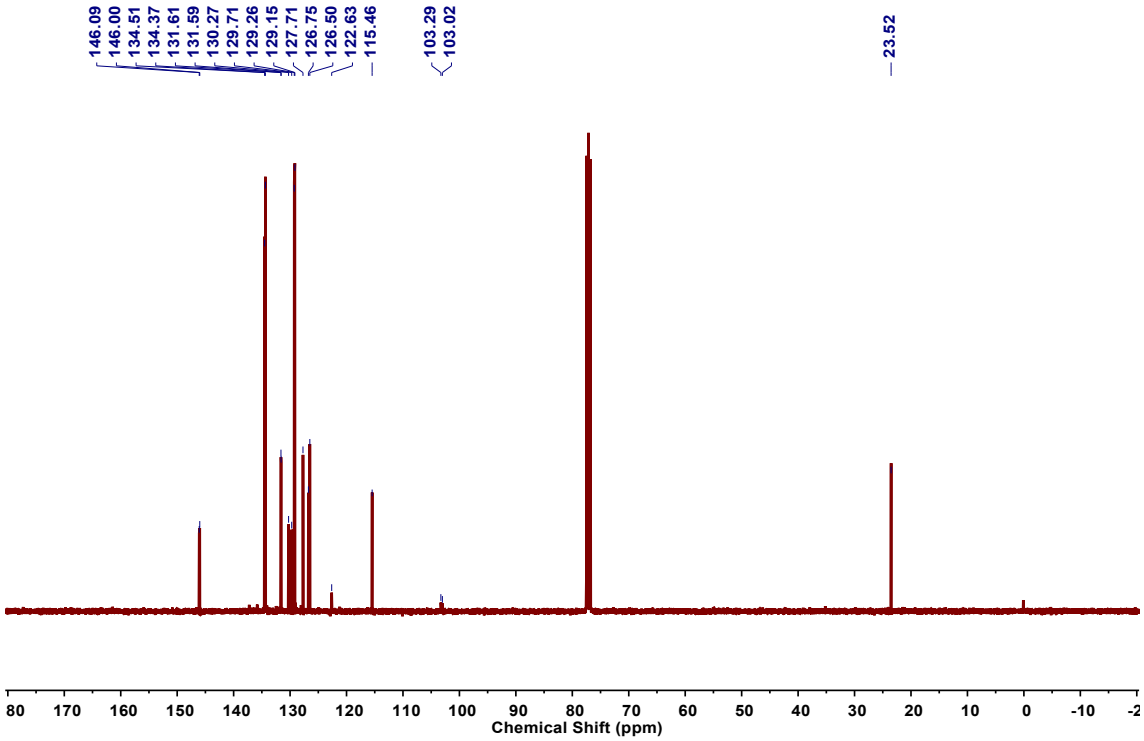

Fig. S49 ^{13}C NMR spectrum (100 MHz, $CDCl_3$, 298 K) of **1c**.

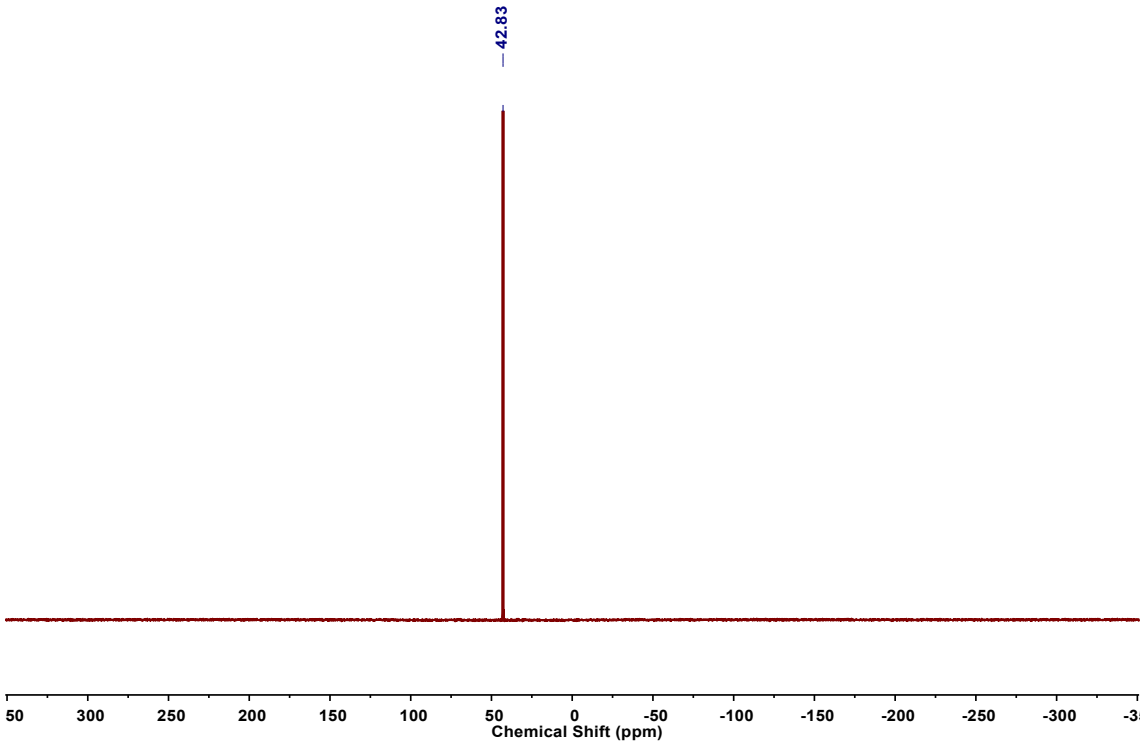

Fig. S50 ^{31}P NMR spectrum (162 MHz, $CDCl_3$, 298 K) of **1c**.

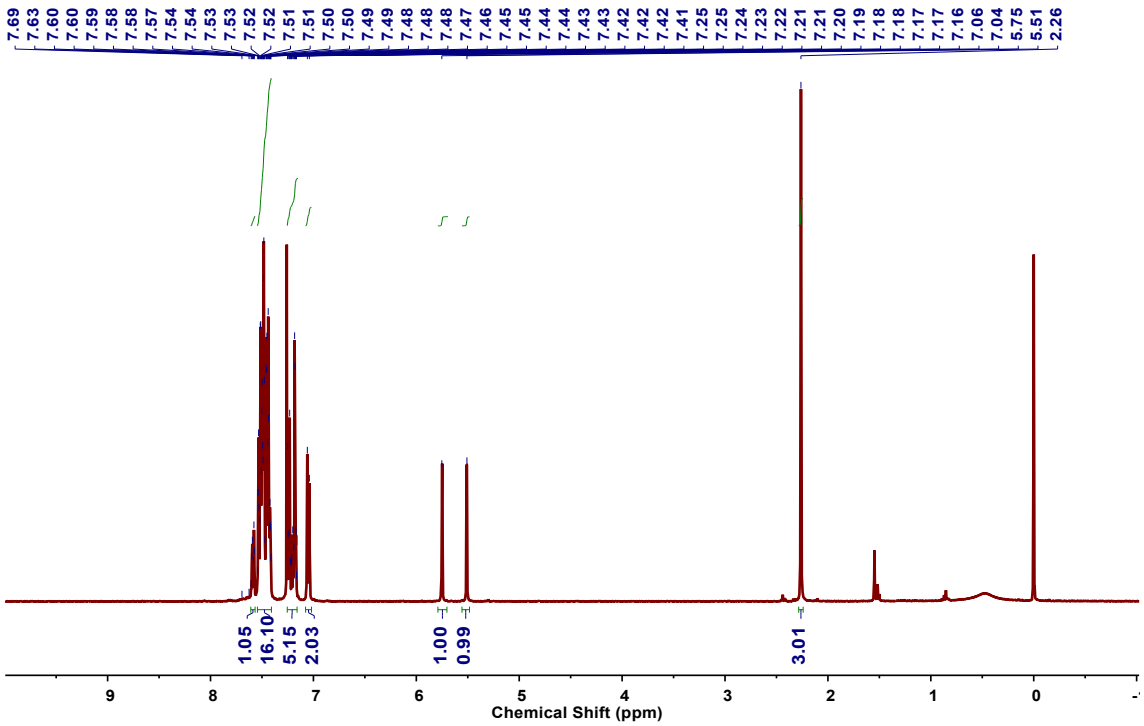

Fig. S51 ^{1}H NMR spectrum (400 MHz, $CDCl_3$, 298 K) of **1b'**.

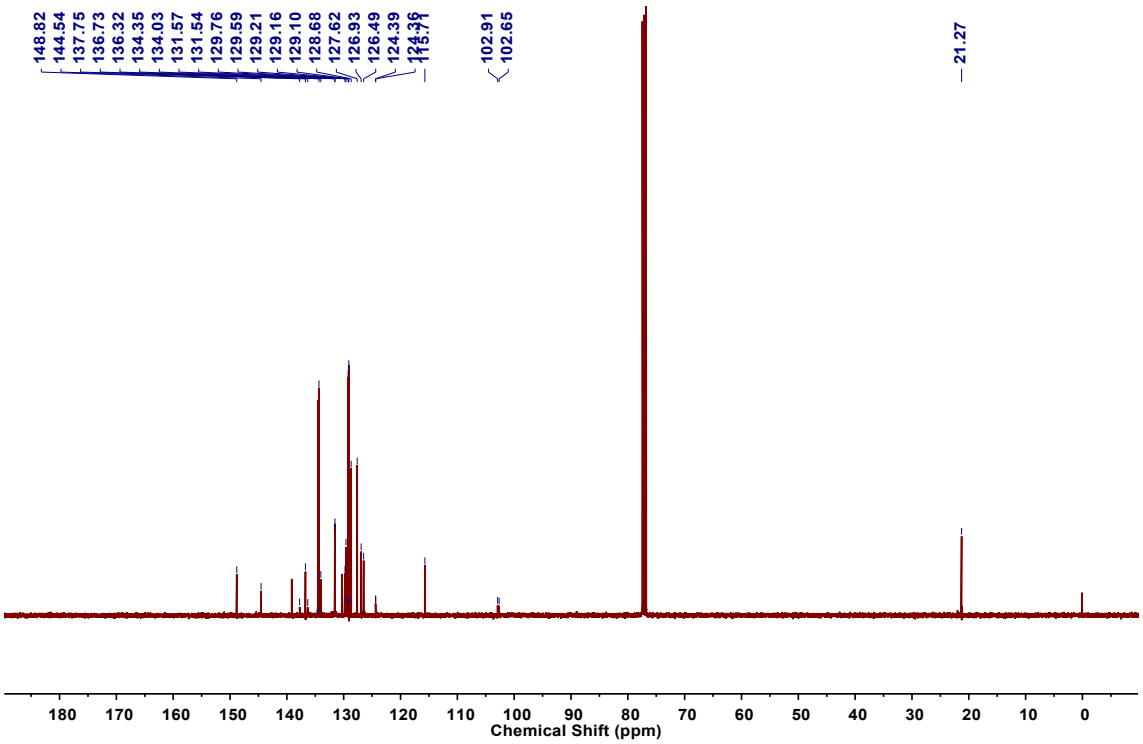

Fig. S52 ^{13}C NMR spectrum (100 MHz, $CDCl_3$, 298 K) of **1b'**.

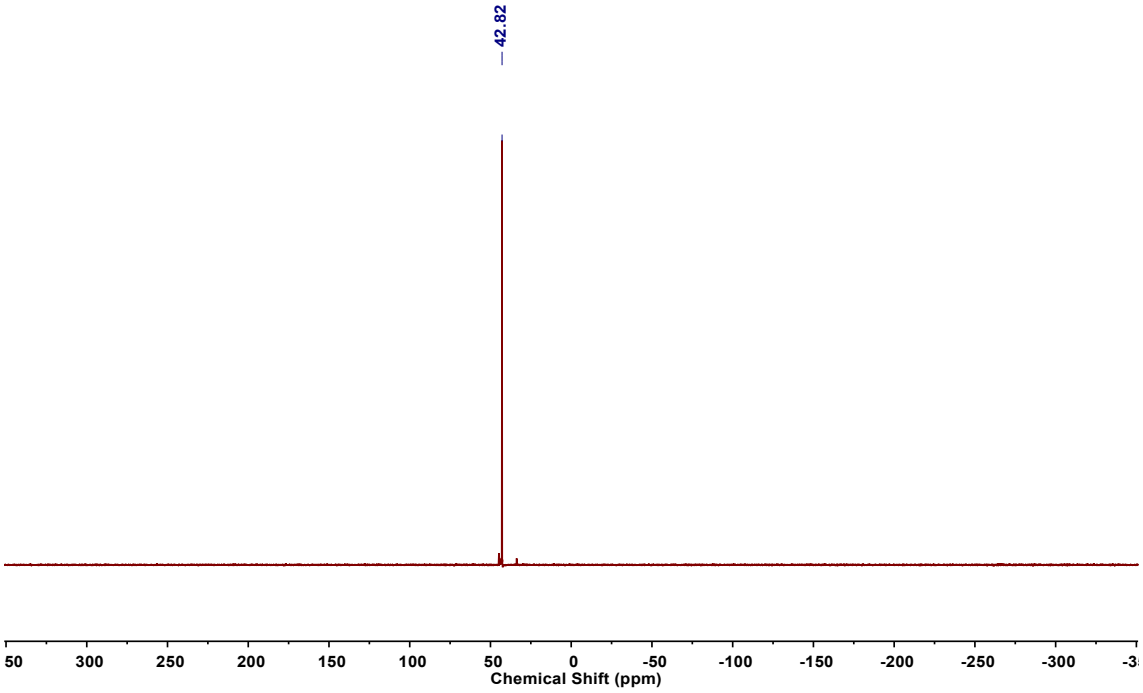

Fig. S53 ^{31}P NMR spectrum (162 MHz, $CDCl_3$, 298 K) of **1b'**.

Supplementary References.

1 Y. Suzuki, S. Naoe, S. Oishi, N. Fujii and H. Ohno, *Org. Lett.*, 2012, **14**, 326-329.

2 R. K. Mohamed, S. Mondal, J. V. Guerrera, T. M. Eaton, T. E. Albrecht-Schmitt, M. Shatruk and I. V. Alabugin, *Angew. Chem. Int. Ed.*, 2016, **55**, 12054-12058.

3 S. V. Gagnier and R. C. Larock, *J. Am. Chem. Soc.*, 2003, **125**, 4804-4807.

4 J. Aziz, G. Frison, P. Le Menez, J.-D. Brion, A. Hamze and M. Alami, *Adv. Synth. Catal.*, 2013, **355**, 3425-3436.

5 S. García-Rubín, C. González-Rodríguez, C. García-Yebra, J. A. Varela, M. A. Esteruelas and C. Saá, *Angew. Chem. Int. Ed.*, 2014, **53**, 1841-1844.

6 K. Shibasaki and H. Togo, *Tetrahedron*, 2021, **79**, 131864.

7 B.-B. Zhu, W.-B. Ye, Z.-T. He, S.-S. Zhang, C.-G. Feng and G.-Q. Lin, *ACS Catal.*, 2021, **11**, 12123-12132.

8 T. Miura and N. Iwasawa, *J. Am. Chem. Soc.*, 2002, **124**, 518-519.

9 G. Sheldrick, *Acta Cryst. A*, 2008, **64**, 112-122.

10 O. V. Dolomanov, L. J. Bourhis, R. J. Gildea, J. A. K. Howard and H. Puschmann, *J. Appl. Cryst.*, 2009, **42**, 339-341.

11 (a) P. van der Sluis and A. L. Spek, *Acta Cryst. A*, 1990, **46**, 194-201; (b) A. Spek, *J. Appl. Cryst.*, 2003, **36**, 7-13.

12 M. E. Casida, *J. Mol. Struct. THEOCHEM*, 2009, **914**, 3-18.

13 P.-F. Li, C.-B. Yi, S.-J. Ren and J. Qu, *Adv. Synth. Catal.*, 2016, **358**, 2088-2092.